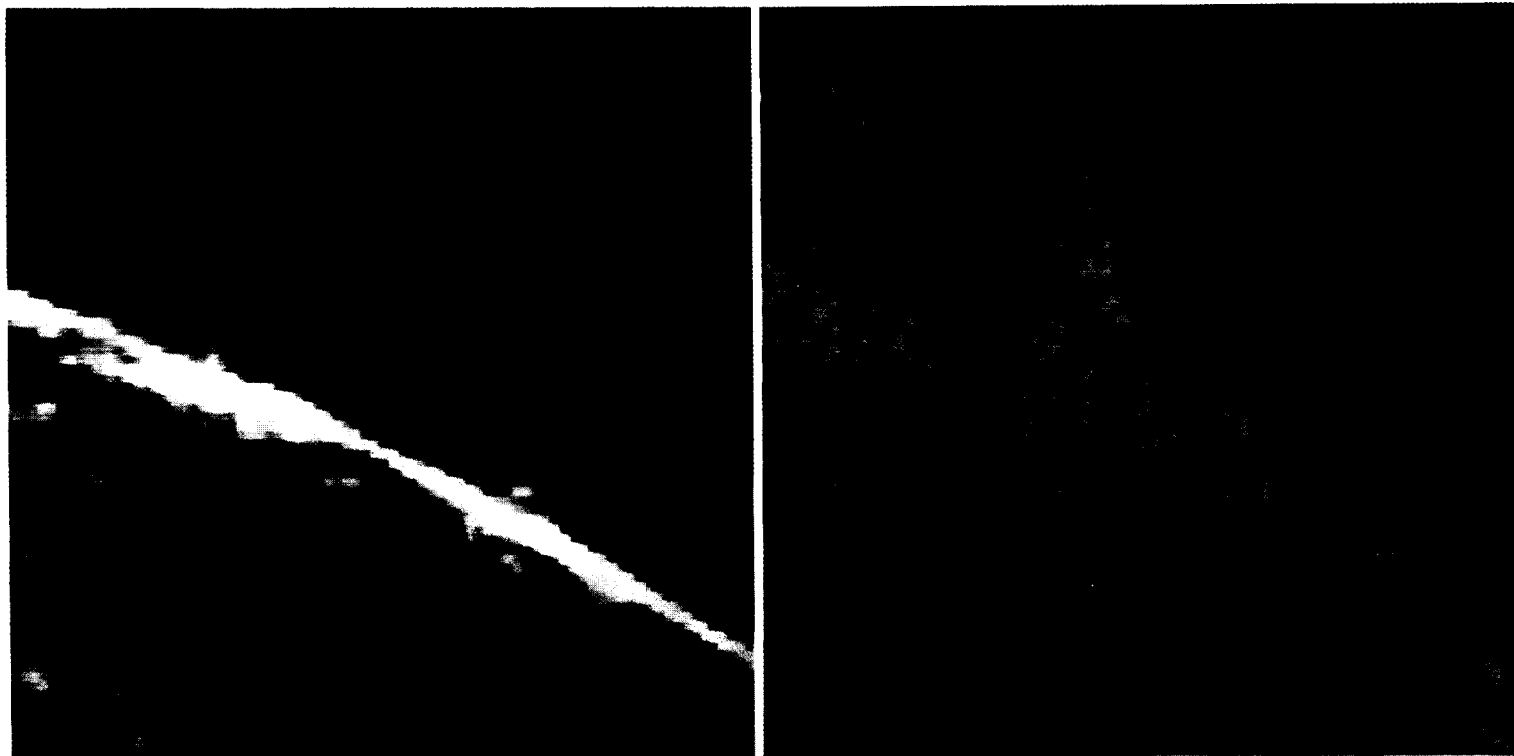


NASA's Solar Maximum Mission: A Look at a New Sun



(NASA-TM-89539) NASA'S SOLAR MAXIMUM
MISSION: A LOOK AT A NEW SUN (NASA) 48 p
Avail: NTIS HC A03/MF A01 CSCL 03B

N87-30245

Unclas
G3/92 0103500

FRONT COVER PHOTOGRAPH:

Intensity and line-of-sight velocity images obtained by the *SMM* Ultraviolet Spectrometer and Polarimeter in the resonance line of C IV at 1548.19 Å. In this observing mode, which employs the Doppler shift of spectral lines to determine relative velocities of emitting plasma along the line of sight, the spectrograph exit slit is bisected by a beamsplitter prism that directs the short- and long-wavelength portions of the line profile to separate detectors. The intensity image (left) is simply the sum of the two signals at each picture element ("pixel"), while the velocity image (right) is given by the ratio of the difference of the signals over their sum. The velocity image is color-coded so that approaching ("blue-shifted") material is shown as blue, and receding ("red-shifted") material is shown as red.

The large loop system extending above the solar limb connects regions of opposite magnetic polarity. Apparently, the loop system is the remnant of an earlier flare that occurred just behind the limb. It is believed that, after plasma heated to tens of millions of degrees K is injected into such loop systems in the brief impulsive phase of a solar flare, the plasma cools radiatively - i.e., by emitting radiation - during the longer gradual phase. Initially, this radiation is characteristically at soft X-ray wavelengths; then, as the material cools, progressively lower-temperature emission is observed. The C IV line is formed at 100,000 K.

NASA's Solar Maximum Mission: A Look at a New Sun

Prepared by
The *SMM* Principal Investigator Teams

Edited by
Joseph B. Gurman

JUNE 1987

DEDICATION

Many of the observations described in this work were obtained in 1984 or later, with the fine-pointed instruments on *SMM*. These data were available only because of the repair of the *SMM* spacecraft by the crew of *Challenger* on mission 41-C. The pilot for that mission, and the commander of *Challenger's* last mission was Francis R. Scobee. This work is dedicated to his memory.

ACKNOWLEDGMENTS

This report would not have been possible without the help of many people associated with the *SMM* project. Drs. E. L. Chupp, B. R. Dennis, A. Hundhausen, R. M. MacQueen, K. J. H. Phillips, O. C. St. Cyr, K. T. Strong, Z. Svestka, E. A. Tandberg-Hanssen, and R. C. Willson all provided text and data, some of it prior to publication in scientific journals. At Goddard, G. Bullock of the Orbiting Satellites Project and T. Smith of the Information Management Division oversaw the printing. I owe a debt of gratitude to all of them, as well as to many scientists, solar forecasters, and mission operations personnel who have contributed to the continuing success of *SMM*.

TABLE OF CONTENTS

	Page
INTRODUCTION	vi
THE SCIENTIFIC HARVEST OF <i>SMM</i>	vii
<i>SMM</i> SCIENCE INSTRUMENTS	ix
GLOSSARY	xii
THE SUN AS A STAR	1
TOTAL SOLAR IRRADIANCE: SOLAR CYCLE AND ACTIVITY-RELATED VARIATIONS	1
HELIOSEISMOLOGY AND THE TOTAL SOLAR IRRADIANCE	1
SOLAR FLARES	5
THE IMPULSIVE PHASE	5
CHROMOSPHERIC EVAPORATION AND THE COOLING PHASE OF FLARES	8
ABUNDANCES, SPECTROSCOPY, AND DIAGNOSTICS	12
ENERGETICS	15
THE ACTIVE SOLAR ATMOSPHERE	17
CORONAL MASS EJECTIONS: STRUCTURE AND FREQUENCY	17
CORONAL MASS EJECTIONS: ORIGIN AND ENERGETICS	19
GLOBAL PROPERTIES OF THE CORONAL MAGNETIC FIELD	22
ACTIVE REGION HEATING	24
PROMINENCE OBSERVATIONS	27
SUNSPOTS	28
NON-SOLAR TARGETS	31
FUTURE PLANS	33

INTRODUCTION

Just as we take the Sun itself almost for granted in our everyday life, despite its vital role in making our planet livable, providing the source of all forms of non-nuclear energy, and governing the circulation of the atmosphere and oceans, astronomers too often overlook the fundamental contributions that the study of the Sun has made in the development of modern astrophysics. Spectroscopy, the basic tool of astrophysics, was first applied to the Sun, as were the atomic physics and energy transport theory that allowed the modeling of stellar atmospheres. Plasma physics, now full of practical applications in devices used to study nuclear fusion, grew in response to the need to understand the ionized, outer regions of the Sun's atmosphere and the earth's magnetosphere, where particle streams from the vicinity of the Sun produce auroral displays. Even the development of nuclear physics was stimulated by the recognition around the turn of the century that a then unknown mechanism provided the energy that fueled the Sun.

More recently, our attempts to understand the physical mechanisms that produce activity cycles (analogous to the 11-year cycle of sunspot number and related activity on the Sun) and heat the tenuous coronae (the outermost atmospheres) of stars with surface temperatures similar to that of the Sun (about 6,000 K) have depended on ever more detailed observations and deeper understanding of the solar paradigms. Indeed, as measurements of the rate of production of the elusive neutrinos in the Sun's thermonuclear core continue to upset our "standard" models of stellar structure and evolution, we have begun to use the global oscillations of the Sun to probe its invisible interior. Even as astronomers look ever farther out to the edge of the universe and the beginning of time, we find ourselves returning again and again to the Sun as our laboratory for understanding how stars work.

As part of this ongoing process of trying to understand the physical processes at work in the Sun, the *Solar Maximum Mission (SMM)* spacecraft was launched on February 14, 1980, near the height of the solar cycle, to enable the solar physics community to examine, in more physically meaningful detail than ever before, the most violent aspect of solar activity: flares. Solar activity fascinates the solar physicist not only because of the solar origin of the magnetic storms that lead to terrestrial aurorae and disrupt telecommunications, but also because sunspots, active prominences, and, above all, flares demonstrate extreme examples of some of the beautiful

variety of physical processes that occur at all times in many classes of astronomical objects.

The *Solar Maximum Mission* began at a time when the solar physics community had had several years to examine the scientific yield of the Apollo Telescope Mount instruments on board *Skylab*. In attempting to understand the physics behind the *Skylab* observations, as well as data from the *Orbiting Solar Observatory (OSO)* series, solar astronomers realized that the wealth of data raised new questions that required a new generation of instrumentation. Some of the questions raised included:

- Coronal loops had been seen to brighten in soft (0.1 – 10 keV) X-ray emission during the later, gradual phase of solar flares, but what occurred during the initial, impulsive phase? Were the impulsive, hard (> 10 keV) X-rays produced at the tops of coronal loops or near the footpoints of the loops in the lower solar atmosphere?
- Were there any systematically observable precursors of flares? Was energy stored in particular structures that were common to most flares?
- How did the matter that emits soft X-rays in flare loops arrive in the loops? Was it in fact evaporated, or ablated, from the much denser regions of the atmosphere at the loop footpoints?
- What was the physical mechanism underlying the original release of energy in a solar flare: the reconnection of magnetic field lines, plasma turbulence, or some other process? Where in the flaring structure did the initial energy release occur?
- How common were γ -ray flares? Where in the solar atmosphere were flare-related γ -rays produced? Were ions and relativistic electrons accelerated in a second stage of flare energy release, after the lower-energy, impulsive-phase electrons had been accelerated?
- What was the response of the transition region between the chromosphere (10^4 K) and the corona (2×10^6 K) to the impulsive phase of flares? Was it possible to measure the magnetic field in the transition region, and did the magnetic field change perceptibly during flares?

- What was the total energy budget of a typical flare – that is, how much energy was radiated at various wavelengths, and how much went into various forms of mechanical energy, such as coronal mass ejections and shock waves? Also, how was the energy released during a flare divided between accelerating particles, heating the ambient plasma, and generating bulk plasma motions?
- On a more fundamental level, did the total solar output vary with the solar activity cycle?

To answer such questions as these, *SMM* was supported by a worldwide observatory coordination known as the Solar Maximum Year (SMY). The *SMM* and SMY observations were coordinated at the *SMM* Experimenters Operations Facility at NASA's Goddard Space Flight Center in Greenbelt, Maryland, where solar physicists from the United States and several European nations gathered to operate their instruments remotely, process the data, and analyze the results. When the spacecraft attitude control system failed in November of 1980, the loss of observations from the pointed instruments was felt worldwide throughout the astronomical community.

The dawning of the Space Shuttle era in 1981 led to new hope for *SMM*: a drive for the repair of the spacecraft in orbit was led by solar physicists, many of whom had no direct connection with the *SMM* program, and by forward-looking members of the aerospace community who saw that an in-orbit repair could initiate a dramatic, new phase of "going to work in space." The *SMM* Repair Mission of April, 1984 – the first retrieval and repair of an orbiting spacecraft – invigorated both the manned space program and solar physics. Just two weeks after the spacecraft was released by the Shuttle, *SMM* instruments observed the most intense flare of the current solar cycle.

THE SCIENTIFIC HARVEST OF *SMM*

The scientific products of *SMM* have been substantial: by 1986, over 400 papers based on *SMM* observations and their interpretation had appeared in scientific journals. More important than such numerical measures of success is the significance of the science that has come from *SMM*. Even a partial compilation serves to indicate the contributions of *SMM* to our understanding of the Sun:

The Sun as a Star

- The total radiant output of the Sun decreased slightly but steadily throughout the first five

years of *SMM*, but has begun to level off as the minimum of solar activity approaches. This may have important implications for our understanding of the processes that govern climate on earth.

- The rotation of large sunspot groups across the visible hemisphere of the Sun is correlated with small but measurable ($\leq 0.25\%$) decreases in the total solar radiative output.
- The frequencies of one class of global solar oscillations have been observed to change slightly, apparently because of solar-cycle-related changes in the outer envelope of the Sun.
- The frequencies of yet another class of global oscillations disagree with those predicted by standard solar models but are better explained by a model including novel physics that would also resolve the solar neutrino problem.

Solar Flares

- Most of the evidence collected by *SMM* indicates that the extremely energetic radiation (hard X-rays and γ -rays) emitted during the brief, violent impulsive phase of solar flares results from the dissipation of the energy in beams of high-energy charged particles accelerated in magnetic loop structures.
- The sizes of those loops are constrained by the very short duration of some of the hard X-ray emission.
- The size of the region in which the particle acceleration takes place is limited by the near-simultaneity of the production of hard X-rays and γ -rays over a broad range of energies.
- In at least some intense flares, high energy mesons and neutrons have been detected at *SMM*. These particles are produced by charged particles which had been accelerated to high energies in the initial stages of the flares.
- Following the impulsive deposition of energy in the denser regions of the solar atmosphere, material from these regions explodes upward into tenuous coronal loop structures at velocities of hundreds of kilometers per second.
- The abundances of certain elements change from flare to flare, and often during the course of individual flares; this indicates that some sort of differentiation mechanism is at work in flares.

- A number of new spectral lines have been identified in the soft X-ray spectra of the unusually hot plasma present in coronal loops during the second, or gradual, phase of flares.
- In some flares, the energy involved in the explosive motions is comparable to the energy in the initial particle beam and the energy radiated in the gradual phase.
- After some major flares, enormous coronal loop structures, persisting for hours, become visible in X-rays.

The Active Solar Atmosphere

- The increase in the rate of coronal mass ejections from solar minimum to solar maximum is less than the corresponding increase in sunspot number, contrary to earlier predictions. What increase there is results from mass ejections at high latitudes.
- At least some coronal mass ejections commence at the time of small X-ray microbursts, and are already under way at the time a true flare occurs in an associated magnetic structure. Such flares should probably be viewed as consequences, rather than causes, of coronal mass ejections. Furthermore, these observations apparently rule out models of mass ejections based on long-lived pressure pulses.
- The rate of change in the angle at which the global coronal magnetic field is tilted with respect to the Sun's rotation axis is approximately twice the value measured during the same phase of the last 11-year solar cycle.

- In at least some parts of active regions, the non-thermal broadening of X-ray spectral lines - thought to be a measure of turbulent motions - is substantial, indicating turbulent velocities of up to 100 km s^{-1} . In addition, in some non-flaring active regions, the X-ray continuum emission can be enhanced for many hours, indicating continuous energy release.
- Dopplergrams (line-of-sight velocity maps) of solar filaments (cool loop structures extending into the hot, tenuous corona) show downflows at the footpoints of the filaments and upward motion in between.
- An *SMM* instrument was able to obtain the first direct measurements of magnetic fields in the transition region, several thousand kilometers above the visible surface of the Sun, the photosphere. (All ground-based magnetic field measurements involving the use of the Zeeman effect are limited to the vicinity of the photosphere.)
- Upward-traveling acoustic waves appear to be a universal feature of the transition region over the dark umbrae of sunspots.

These topics, as well as other findings of *SMM* investigators, are described in more detail in the following sections of this report. Even though *SMM* instruments are so-called "P.I. experiments," designed, constructed, and operated by Principal Investigator teams, much of the scientific analysis of *SMM* data has been performed by Guest Investigators supported by a strong Guest Investigator program. Only through the strength and involvement of the worldwide solar physics community has *SMM* been able to qualify as a scientific success.

SMM SCIENCE INSTRUMENTS

The *Solar Maximum Mission* spacecraft carries the most diverse and sophisticated payload of scientific instruments ever orbited to study solar activity. A brief description of each instrument follows.

Active Cavity Radiometer Irradiance Monitor (ACRIM)

Principal Investigator:
Dr. Richard C. Willson
Jet Propulsion Laboratory
Pasadena, California

The ACRIM (Willson 1979) is a cavity pyrheliometer, with solar input during half of each 131.072 s measurement interval and servo-adjusted heat input during the rest of each cycle, when a shutter blocks the solar input. The solar irradiance at the earth is therefore proportional to the difference between the heating rates with the shutter open and closed. The accuracy of each irradiance measurement obtained in this way is approximately 0.1%.

Coronagraph/Polarimeter (C/P)

Principal Investigator:
Dr. Robert M. MacQueen
High Altitude Observatory
National Center for Atmospheric Research
Boulder, Colorado

The C/P (MacQueen *et al.* 1980) is an externally occulted Lyot coronagraph with a vidicon detector. Images of the corona with 10" spatial resolution are built up in four quadrants by means of sector mirrors. In addition, with seven filters (including ones centered on the Fe XIV "green line" at $\lambda 5303 \text{ \AA}$ and H α) and three polaroids with principal axes 60° apart, the C/P is able to obtain measurements of coronal electron densities and distinguish ejected material at chromospheric temperatures from coronal features. A fully independent pointing control system allows the C/P to observe independently of the solar feature pointing of the *SMM* spacecraft.

Shortly before the *SMM* attitude control system (ACS) failed in 1980, an electronic component in the C/P Main Electronics Box (MEB) failed; C/P was no longer able to image the solar corona. Unlike the ACS module, the MEB was neither mounted externally nor designed to be replaced in orbit. The *SMM* Repair Mission team, however, developed new hardware and new methods that allowed astronauts George Nelson and James van Hoften to replace the MEB with a new unit. C/P has been operating successfully since the *SMM* repair.

Gamma Ray Spectrometer (GRS)

Principal Investigator:
Dr. Edward L. Chupp
University of New Hampshire
Durham, New Hampshire

The GRS (Forrest *et al.* 1980) includes seven integral-line calibrated NaI(Tl) detectors for nuclear lines between 0.3 and 0.9 MeV; the energy resolution (full width at half maximum) of these detectors is better than 7% at 0.662 MeV. In addition, a thick CsI(Na) crystal, along with the NaI(Tl) spectrometers, is sensitive to γ -rays in the range 10–140 MeV, and neutrons with energies above 20 MeV. Finally, an auxiliary system of two NaI detectors yields hard X-ray fluxes from 10 to 140 keV. Time resolutions are typically about 2 s and 16 s, but can be as fine as 64 ms for the 300–350 keV energy band. Since the field of view is close to half the sky, GRS has observed approximately as many cosmic as solar events, and sweeps across the galactic center each year as *SMM* follows the Sun.

Hard X-Ray Burst Spectrometer (HXRBS)

Principal Investigator:
Dr. Brian R. Dennis
NASA Goddard Space Flight Center
Greenbelt, Maryland

The HXRBS (Orwig *et al.* 1980) was designed to examine the role of energetic electrons in solar flares. Scintillation events in its actively collimated CsI(Na) detector are read out every 128 ms in fifteen energy channels between ~ 25 to ~ 500 keV. A circulating memory is able to accumulate relatively brief periods of data during the more intense flares with time resolution down to 1 ms. The full width at half maximum of the field of view is approximately 40°.

Hard X-Ray Imaging Spectrometer (HXIS)

Principal Investigator:
Prof. C. de Jager
Space Research Laboratory
The Astronomical Institute at Utrecht
The Netherlands

The HXIS (Van Beek *et al.* 1980), a joint project of the Space Research Laboratory (Utrecht) of the Netherlands and the Department of Space Research of the University of Birmingham, U.K., consists of an imaging collimator of ten grid plates, each divided into 576 sections, and a position-sensitive detector

system consisting of 900 mini-proportional counters. The grids form a coarse field of view $6'24''$ in extent (with $32''$ square picture elements, or "pixels") and a fine field of view $2'40''$ across (with $8''$ square pixels). Each pixel is sampled in six energy bands ranging from 3.5 to 30 keV, with time resolution down to 1.25 s. HXIS was able to send the other *SMM* instruments a "flare flag" message via the spacecraft on-board computer when an adjustable number of counts in a given energy range occurred in any single pixel. This flare flag, which could be set to different levels for different recipient instruments, allowed the other instruments to repoint or recenter their raster mechanisms and provide the rapid response necessary to capture the impulsive phase at the beginning of most solar flares.

After nine months of active operation, the second redundant HXIS microprocessor failed soon after the *SMM* attitude control system failure, and it was no longer possible to recover data from the instrument. Although the possibility of replacing the microprocessor during the 1984 *SMM* repair mission was investigated, this option had to be rejected because the HXIS electronics were not accessible without risking damage to components of other instruments. The 1980 HXIS data set, however, forms a most impressive record of the spatial and energetic distribution of X-rays in solar flares, with a spatial resolution never before achieved at such high energies.

Ultraviolet Spectrometer and Polarimeter (UVSP)

Principal Investigator:

Dr. Einar Tandberg-Hanssen
NASA Marshall Space Flight Center
Huntsville, Alabama

The UVSP (Woodgate *et al.* 1980), a joint project of the NASA Marshall and Goddard Space Flight Centers, consists of an aplanatic Gregorian telescope of approximately $2''$ resolution, an Ebert-Fastie spectrometer, and five photomultiplier detectors (four CsI photocathode tubes for use below 1900 Å and one CsTe tube for use at longer wavelengths). The telescope secondary is mounted on gimbals and may be rastered to build up an image of an area on the Sun of up to $256'' \times 256''$, in steps of as little as $1''$. In a pivoting slit wheel are 22 combinations of entrance aperture and diametrically opposed exit slits (as many as five exit slits per aperture). The entrance apertures range in size from $1'' \times 1''$ to $15'' \times 286''$, and the exit slits range from 0.01 to 3.0 Å in second order. Several of the exit slits are bisected by beam splitter prisms that can direct the short- and long-wavelength sides of a line profile to different detectors to allow velocity imaging ("Dopplergrams")

of selected areas of the solar surface. A polarimeter may be inserted behind the exit aperture; it consists of two systems: a three-quarter wave retarder for those wavelengths where the spectrograph grating is an effective linear polarizer, and a quarter-wave retarder and linear polarizer for use at wavelengths at which the grating polarization is very low. The instrument is sensitive to wavelengths of 1170–1800 Å in second order and up to 3600 Å in first order. All instrument functions are controlled by a small, dedicated computer.

In April, 1985, the UVSP grating drive mechanism became stuck; efforts to release the obstruction were unsuccessful, and apparently led to the failure of a coupling in the drive in September, 1985. The grating appears to be fixed at a wavelength of ≈ 1380 Å (second order; ≈ 2760 in first order). During periods of solar activity, UVSP is used in second order to provide pointing and timing information for use in conjunction with other *SMM* instruments; at other times, first-order measurements of ozone concentration in the earth's atmosphere are carried out at spacecraft sunrise and sunset. These unique observations are making possible a mapping of ozone concentrations at latitudes of -50° to 50° at altitudes of 50–75 km.

X-Ray Polychromator (XRP)

Principal Investigators:

Dr. J. Leonard Culhane
Mullard Space Science Laboratory
University College London
United Kingdom

Dr. Kenneth J. H. Phillips
Rutherford Appleton Laboratory
United Kingdom

Dr. Keith T. Strong
Lockheed Palo Alto Research Laboratories
Palo Alto, California

The XRP (Acton *et al.* 1980), a joint project of the three institutions of the Principal Investigators, consists of a Flat Crystal Spectrometer (FCS) and a Bent Crystal Spectrometer (BCS). The FCS is able to rotate its crystals to provide its seven detectors with access to the spectral range 1.40–22.43 Å. In addition, the FCS can be rastered to build up images with $\approx 14''$ resolution. The FCS detectors are proportional counters with either sealed beryllium windows (the three shortest wavelength detectors) or thin polypropylene windows with an active propane gas system. The BCS, with a collimator field of view of $6'$, is able to obtain spectra in the range 2–3 Å, with a resolution $\lambda/\Delta\lambda$ of $\approx 10^4$, with eight position-sensitive proportional

counters. Each instrument is controlled by a micro-processor. At this writing, six BCS and five FCS detectors are still functional.

References

Acton, L. W. *et al.* 1980, *Solar Physics*, 65, 53

Forrest, D. J. *et al.* 1980, *Solar Physics*, 65, 15

MacQueen, R. M., Csoeke-Poeckh, A., Hildner, E.,

House, L., Reynolds, R., Stanger, A., Tepoel, H., and Wagner, W. 1980, *Solar Physics*, 65, 91

Orwig, L. E., Frost, K. J., and Dennis, B. R., 1980, *Solar Physics*, 65, 25

Van Beek, H. F., Hoyng, P., LaFleur, B., and Simnett, G. M. 1980, *Solar Physics*, 65, 39

Willson, T. C. 1979, *Applied Optics*, 18, 179

Woodgate, B. E. *et al.* 1980, *Solar Physics*, 65, 73

GLOSSARY

ACRIM	The Active Cavity Radiometer Irradiation Monitor on <i>SMM</i> . This instrument uses a black-body cavity to measure the total irradiance of the visible hemisphere of the Sun.
arcade	A series of magnetic loops, overlying the magnetic neutral line in a solar active region.
arc sec	Arc second ($''$), a common measure of angular size on the solar disk. At disk center, $1''$ corresponds to ≈ 725 km. 60 arc sec = 1 arc minute ($1'$).
BCS	The Bent Crystal Spectrometer of the X-Ray Polychromator on <i>SMM</i> . This coarsely collimated instrument with a $6'$ field of view is capable of obtaining high-resolution soft X-ray spectra in the region of $2-3 \text{ \AA}$, which contains the resonance lines of Fe XXV, Fe XXVI, and Ca XIX.
CFOV	The coarse field of view of the Hard X-ray Imaging Spectrometer (HXIS); $6'24''$ across, with $32'' \times 32''$ pixel size.
C/P	The Coronagraph/Polarimeter on <i>SMM</i> . This instrument consists of an externally occulted coronagraph with polarizing, $H\alpha$, and Fe XIV filters.
CME	Coronal Mass Ejection - a transient outflow of plasma, at velocities up to several hundred km s^{-1} , in the tenuous solar corona.
degree	In global stellar oscillations, the number ℓ of circles on the stellar surface where the velocity vanishes.
faculae	Small knots of emission observed in chromospheric emission lines (and in integrated white light near the limb.)
FCS	The Flat Crystal Spectrometer of the X-Ray Polychromator on <i>SMM</i> . This instrument is capable of both spatial rastering to build up images with $14''$ resolution, and crystal scanning to build up spectra in soft X-rays at $1.40 - 22.43 \text{ \AA}$.
FFOV	The fine field of view of the Hard X-ray Imaging Spectrometer (HXIS); $2'40''$ across, with $8'' \times 8''$ pixel size.
footpoints	The locations at which magnetic loops are anchored in the lower solar atmosphere.
g-modes	Gravity modes - eigenmodes of global oscillations in which buoyancy is the restoring force.
gradual phase	The longer (10 minutes to 2 hours), second phase of most solar flares, following the impulsive phase (<i>q.v.</i>), the gradual phase is characterized by slowly rising, then falling, soft X-ray emission.

GRS	The Gamma-Ray Spectrometer on <i>SMM</i> , sensitive to photons with energies of 10 keV to 140 MeV and neutrons with energies over 20 MeV.
HXIS	The Hard X-ray Imaging Spectrometer on <i>SMM</i> . This instrument was able to obtain the first images of solar flares at energies of 3.5 to 30 keV.
HXRBS	The Hard X-Ray Burst Spectrometer on <i>SMM</i> . This instrument has been used to measure full-Sun hard X-ray fluxes in 15 energy bands between ~ 25 and ~ 500 keV with time resolution up to 1 ms, for over 8000 flares.
impulsive phase	The brief (10 s - 10 m) initial phase of most solar flares, characterized by rapidly varying hard X-ray, γ -ray, radio, and ultra-violet emission.
loops	Arches of magnetic flux extending above the visible solar atmosphere; these are believed to be the location of the primary release of flare energy.
order	Radial order - in global stellar oscillations, the number of nodes (points at which the velocity vanishes) along a stellar radius.
p-modes	Pressure modes - eigenmodes of global oscillations in which pressure is the restoring force.
reconnection	The realignment of magnetic field lines to a lower energy state; a candidate mechanism for the initial source of flare energy.
UVSP	The UltraViolet Spectrometer and Polarimeter on <i>SMM</i> . This instrument operates with high spectral resolution in the range 1170 - 3600 Å and spatial resolution of 2".
XRP	The X-Ray Polychromator on <i>SMM</i> . This experiment consists of the BCS and FCS (<i>q. v.</i>).

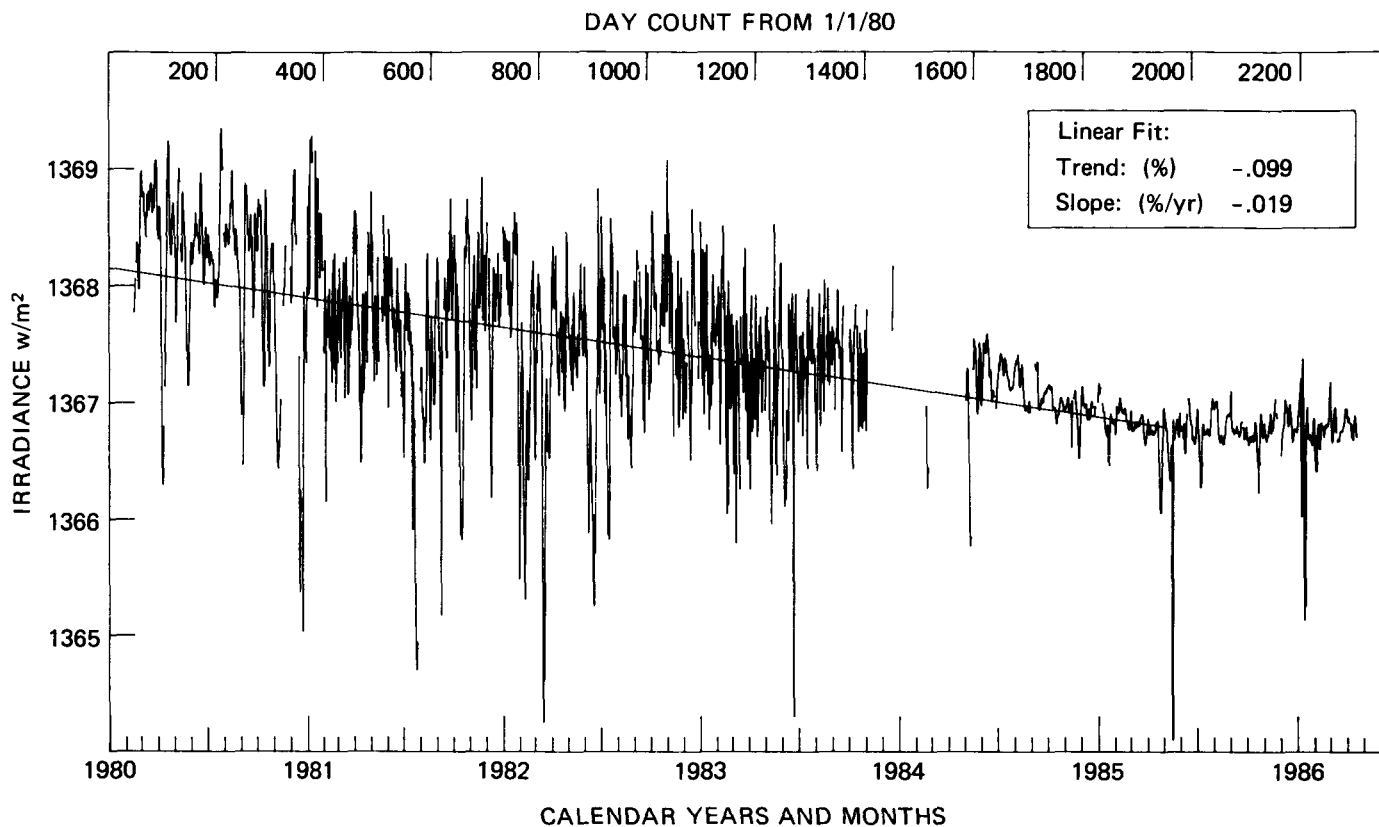


Figure 1. Time series of ACRIM daily mean results for the 1980-1986. Standard errors of the daily means increased from 10^{-4} to 5×10^{-4} during 1981-83 due to a much lower rate of data acquisition during this period of coarse stabilization of the *SMM* spacecraft. (The primary attitude control system, based on rate wheels, was out of service due to an electronic failure, but a backup system based on magnetic torquers kept the spacecraft pointing to within a few degrees of the Sun. As a result, *SMM*'s solar panels were fully illuminated, but pointed instruments were unable to obtain data.) All the prominent downward "spikes" correspond to the passage of active regions containing large sunspot groups across the visible hemisphere of the Sun. Some of the upward spikes may be associated with bright faculae in the active regions.

A linear least-mean-squares fit to the irradiance measurements through early 1985 yields a slope of $-0.019\% \text{ yr}^{-1}$, and a net change of about 0.1%. Independent total solar irradiance observations by sounding rocket, balloon, and *Nimbus 7/ERBS* experiments show generally good agreement with these ACRIM results, with a linear least-mean-squares fit slope of $-0.014\% \text{ yr}^{-1}$. In the last two years, however, the mean irradiance has flattened out, prompting speculation that solar luminosity and solar activity are correlated. If this correlation is supported by an increase of the total solar irradiance as we approach the next solar maximum, we will need to explore basic solar physical processes to explain this aspect of the solar activity cycle. It may even be possible that a similar decrease in solar output at low solar activity levels was responsible for the "little ice age" during the prolonged Maunder sunspot minimum of the late 17th and early 18th centuries, when the solar cycle was apparently inactive for over four decades.

of the Sun) rather than the strong increase of temperature with decreasing radius in the standard model. Since the rate of neutrino production from ${}^8\text{B}$ decay (i.e., those neutrinos currently observable) is very sensitive to temperature, the neutrino production rate predicted by a WIMPy solar model is low enough to match the observed rate (Gilliland *et al.* 1986). In such a model, then, the temperature, density, and mean molecular weight differ from those in a standard model. As a result, the sound speed will differ as well, and the eigenfrequencies of global modes will differ from those predicted by a

standard model. Since the amplitude of most p-modes is negligible in the deep interior, their frequencies are changed only slightly by a WIMP model. The g-modes, however, are strongest at small r , and the frequency separation of low-degree, high-order g-modes - 29 minutes (Faulkner *et al.* 1986) or 33 minutes (Däppen *et al.* 1986) - is significantly less than the 36.8 minute value predicted by standard models. Results of a preliminary analysis of ACRIM data (Fröhlich 1986) are best fit with a fundamental g-mode period spacing of 29.8 minutes.

Finally, on time scales of a few minutes, ACRIM data have provided the first observations of the global solar p-mode oscillations from a spacecraft. In particular, ACRIM measurements in 1980 of low-degree ($\ell = 0, 1,$ and 2) modes with periods around 5 minutes show no evidence of splitting in the $\ell = 1$ modes, and thus provide no evidence for rapid rotation of the Sun's core (Woodard and Hudson 1983). Comparison of 1980 and 1984 measurements of radial order $n = 17$ to 26 modes (Woodward and Noyes 1985) reveals a mean decrease in frequency of $(0.42 \pm 0.14) \mu\text{Hz}$. If ACRIM observations continue through the solar cycle, investigators may be able to determine whether the solar cycle modulates the eigenfrequencies through cycle-dependent changes in granulation and supergranulation, magnetic field, or turbulent velocities in the convection envelope.

A second ACRIM flight experiment is presently being prepared for launch in 1989. A continuous solar irradiance record with precision adequate for both climatology and helioseismology requires overlapping observations by both ACRIMs.

References

- Däppen, W., Gilliland, R. L., and Christensen-Dalsgaard, J. 1986, *Nature*, 321, 229
- Faulkner, J., Gough, D.O., and Vahia, M. N., *Nature*, 321, 226
- Fröhlich, C. 1986, in preparation
- Gilliland, R. L., Faulkner, J., Press, W. H., and Spergel, D. N. 1986, *The Astrophysical Journal*, 306, 703
- Willson, R. C. 1982, *Journal of Geophysical Research*, 87, 4319
- Willson, R. C. 1984, *Space Science Reviews*, 38, 222
- Willson, R. C., Gulkis, S., Janssen, M., Hudson, H. S., and Chapman, G. A. 1981, *Science*, 211, 700
- Woodward, M. and Hudson, H. S. 1983, *Nature*, 305, 589
- Woodward, M., and Noyes, R. W. 1985, *Nature*, 318, 449

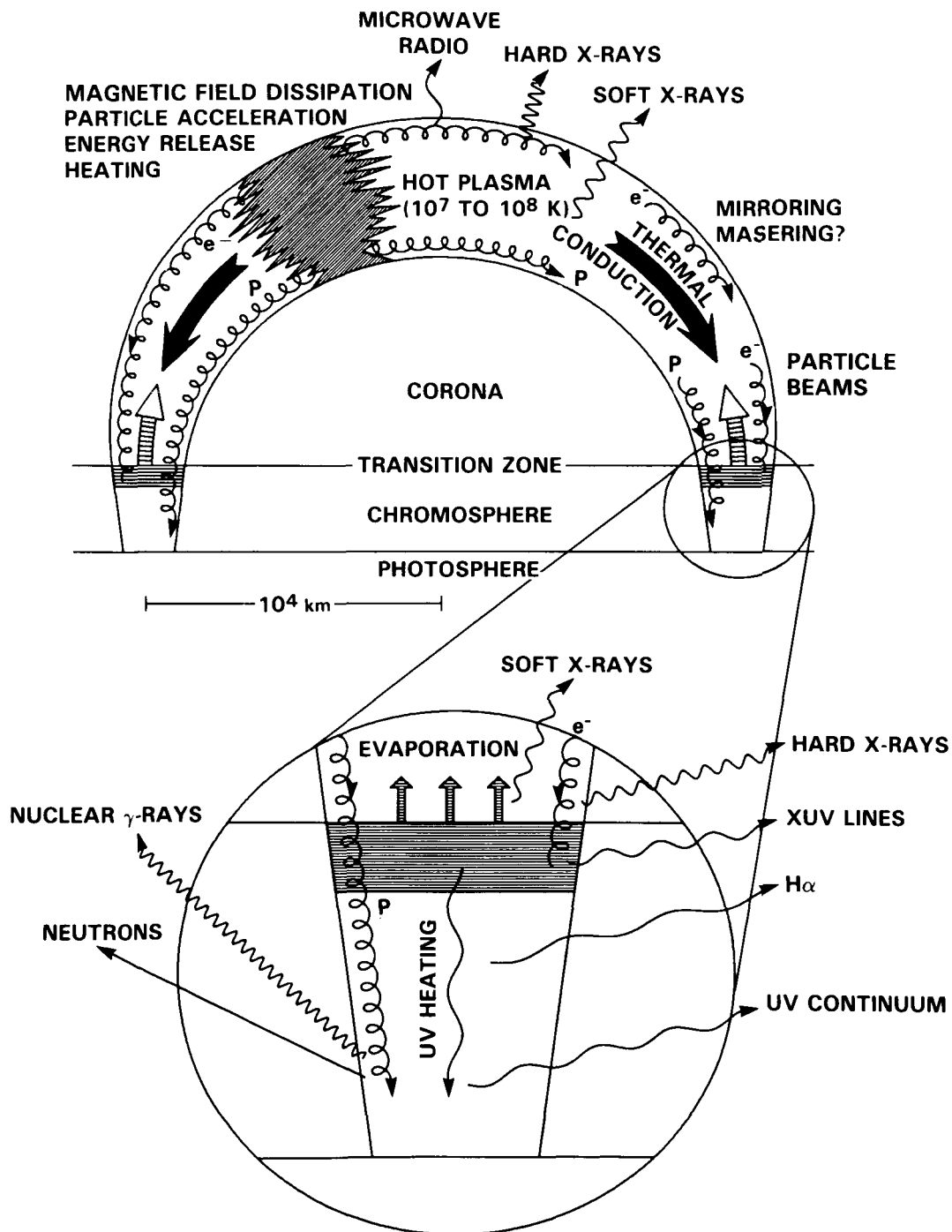


Figure 2. A possible flare scenario, consistent with a wide range of observational data: Although a single loop structure is shown in cross-section, much more complicated field geometries are common. As a result of the dissipation of magnetic energy by an as yet ill-defined mechanism, electrons and protons are impulsively accelerated, probably in the coronal regions of the loop. These particles subsequently propagate along the magnetic field lines and interact with the ambient plasma in the legs of the loop and at the footpoints. Hard X-rays, γ -rays, microwave radio emission, and neutrons are produced during this "impulsive" phase. At the loop footpoints, the particle beam is thermalized: its energy is converted to heat in the denser plasma of the lower corona, transition region, and chromosphere. Although this excited plasma emits radiant energy at a variety of wavelengths, radiative losses do not remove the excess thermal energy fast enough, and explosive "evaporation" of chromospheric material occurs. This material has been heated to temperatures of tens of millions of degrees K, and cools slowly by radiation (of soft X-rays) and conduction during the "gradual" or cooling phase as it fills the large loop structures.

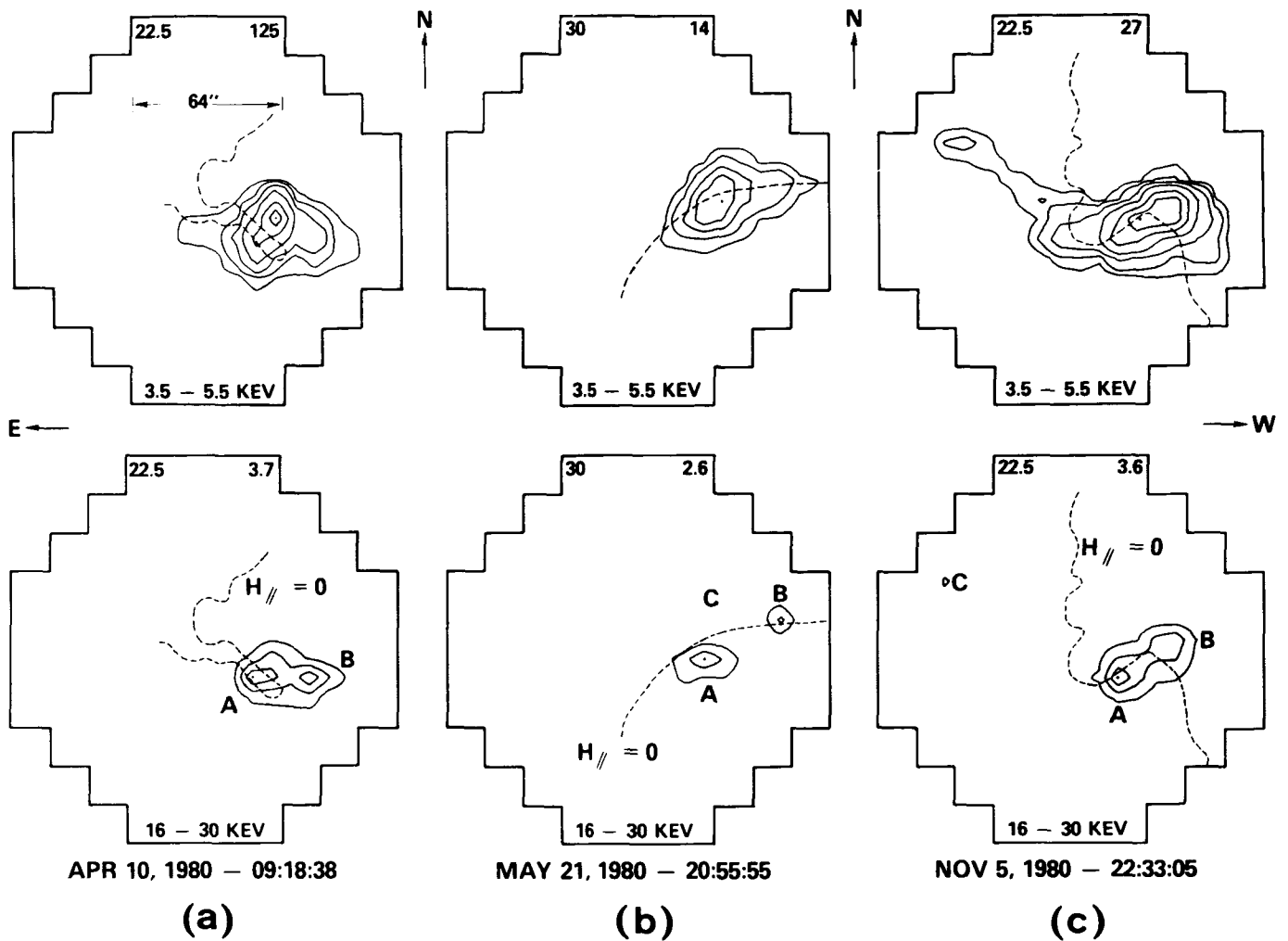


Figure 3. Contour plots in soft (3.5–5.5 keV, above) and hard (16–30 keV, below) X-rays at the onset of the impulsive phase of three major flares (from Duijveman *et al.* 1982). The frames represent the fine field of view (FFOV) of HXIS, with the scale indicated in the upper left picture. The dashed lines show the neutral line between opposite magnetic polarities.

longer than observed if the flare loops are large enough to produce the observed hard X-ray fluxes.

The observation by HXRBS that spikes in the impulsive hard X-ray emission can be as brief as 45 milliseconds (Kiplinger *et al.* 1983) also constrains the thick-target model to loops of half-length less than 12,000 km. Kiplinger *et al.* point out, however, that the loop length could be longer if the initial pitch angle distribution for the particle stream is highly anisotropic.

A further constraint on the process responsible for the acceleration of charged particles to mildly relativistic energies in the impulsive-phase of solar flares comes from data obtained by both GRS (Forrest and Chupp 1983) and the Japanese *Hinotori* spacecraft (Yoshimori *et al.* 1983). The onset of impulsive-phase emission is simultaneous (to within measurement uncertainties of 0.8–2.0 s) for photon energies of 40 keV to 6.4 MeV. This implies that all

the accelerated particles, regardless of energy, are interacting with the “target” (the denser layers of the active region atmosphere) simultaneously. In contrast, the peak of impulsive phase emission occurs 2 s or more later at the highest γ -ray energies ($E > 4$ MeV) than in hard X-rays, and this delay may be explained by energetic particles leaking out of a magnetic trap.

Another intriguing GRS observation is shown in Figure 4, which depicts the photon spectrum during the 65 s impulsive phase of a flare. The “hardening” (shoulder) at energies above 40 MeV may be explained by the superposition of a bremsstrahlung power-law (straight-line) spectrum and a neutral pion (π^0) photon spectrum. The neutral pions are the products of nuclear collisions between ions accelerated in the flare and the ions in the denser regions of the solar atmosphere. Since the γ -rays identified with π^0 decays in this event persisted for

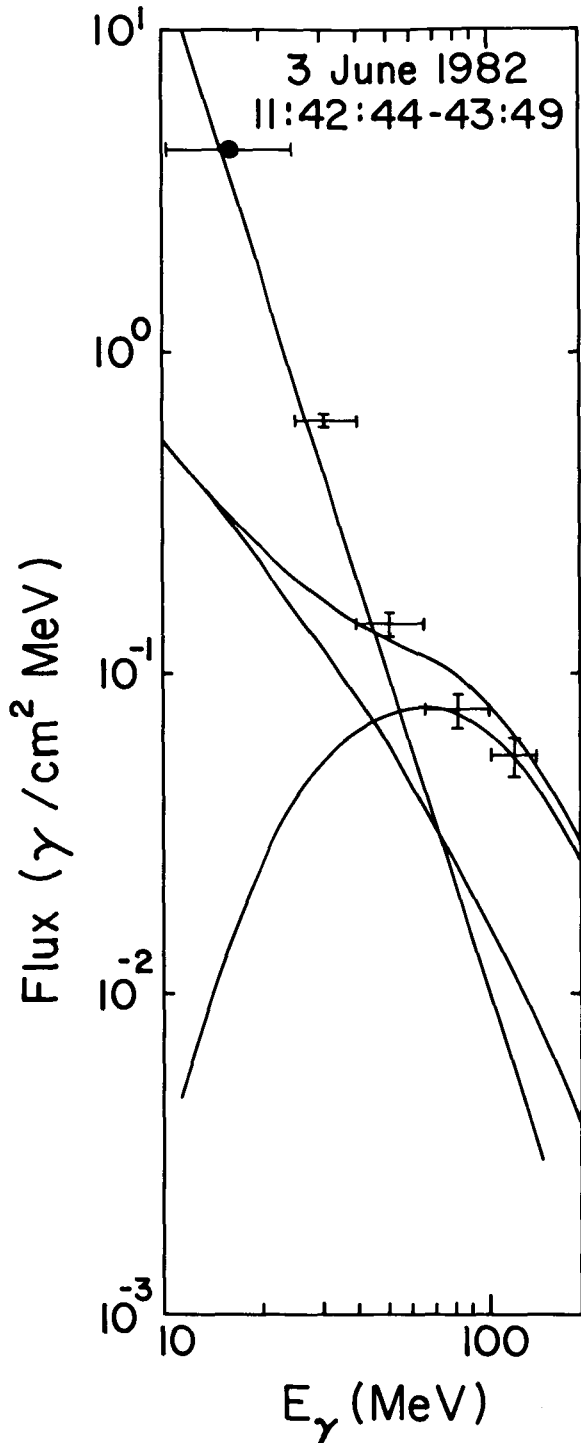


Figure 4. GRS measurements (error bars) of the 10 - 140 MeV γ -ray spectrum from the impulsive phase of the June 3, 1982 flare. The observations are consistent with a sum of an electron bremsstrahlung power-law spectrum (straight line) and a π^0 decay spectrum (arc peaking at ~ 70 MeV).

~ 30 minutes, the short pion lifetime ($\sim 10^{-15}$ s) implies that ion acceleration continues for up to half an hour after the impulsive phase of some flares.

One of the most startling discoveries by *SMM* is the observation by GRS of neutrons of energies up to ≈ 1 GeV. The neutrons are released during the impulsive phase of large flares, but their arrival at the earth trails that of the impulsive phase γ -ray emission by up to ≥ 1000 seconds, with the delay depending on the neutron energy (Chupp *et al.* 1982, Chupp 1984) - see Figure 5. Since GRS has observed impulsive phase photons with energies greater than 50 MeV, and neutrons with energies up to 1 GeV, either an effective particle accelerator is operative during the relatively brief impulsive phase of flares, or preaccelerated particles are released impulsively into a target during the impulsive phase.

CHROMOSPHERIC EVAPORATION AND THE COOLING PHASE OF FLARES

Soon after the initial release of energy in the impulsive phase, the downward-streaming particles are thermalized, and the hard X-ray emission spreads over the whole coronal loop. A comparison of HXIS and XRP data yields results consistent with a model in which the energy deposited in the chromosphere by the energetic particle streams can only be released thermodynamically by the ablation ("evaporation") of chromospheric gas, followed by the explosive rise of the heated plasma into large but previously tenuous active region coronal loops as the chromosphere is pushed downward (Gunkler *et al.* 1984). This process, or a variation of it, is commonly referred to as chromospheric evaporation. The BCS has observed a large number of flares that show a characteristically blue-shifted component in soft X-ray spectral lines (Figure 6), which is interpreted as evidence for the upward motion of the exploding chromospheric material (Antonucci and Dennis 1983). At least some of the expansion is horizontal, since in at least two cases, strong flares on the solar limb displayed line profiles with separate components on the short-wavelength side (Bentley *et al.* 1986). In one of these cases, the blueshift was 370 km s^{-1} (see Figure 5).

Intense turbulence during the impulsive onset of flares is also revealed by the broadening of the same spectral lines (Figure 7). These mass motions have been observed almost exclusively in the high temperature ($T_e \geq 10^7$ K) lines of Ca XIX and Fe XXV as seen by the *P78-1* spacecraft (Doschek *et al.* 1979) and BCS. This leaves open the question of the importance of mass motions in the lower temperature coronal plasma ($T_e \leq 5 \times 10^6$ K), which contains the bulk of the thermal energy in a flare. Preliminary results from FCS observations indicate that equivalent mass motions also occur in the cooler plasma.

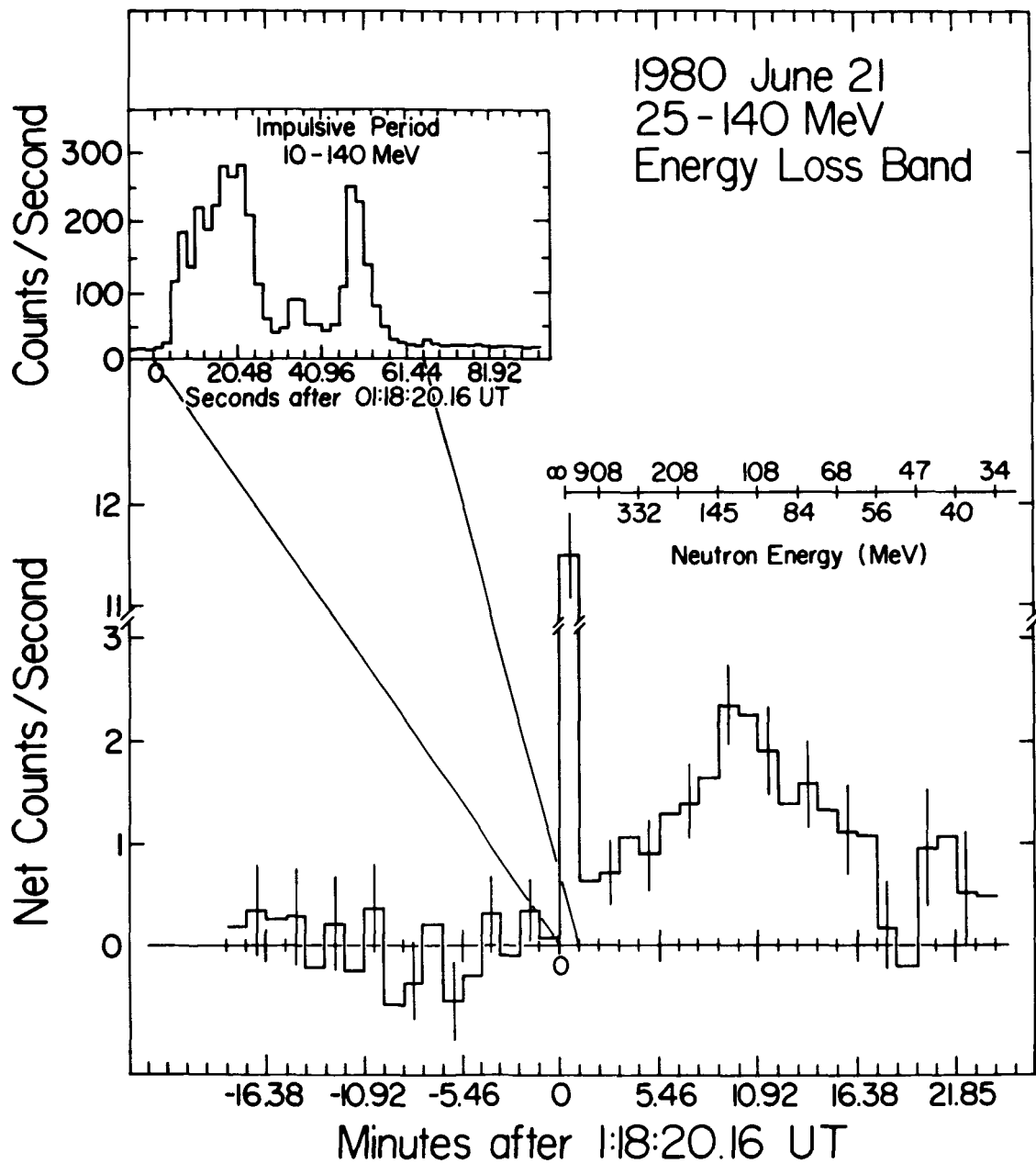


Figure 5. The arrival time history of energetic (> 25 MeV) γ -ray photons and neutrons at the vicinity of the earth in the intense flare of 21 June, 1980, as recorded by GRS.

Little was known about the location of the burst sites where chromospheric evaporation is believed to take place, until *SMM* provided simultaneous hard X-ray and UV images of such events. In at least some such events, brightenings occur at several locations within the active region during the initial stages of a flare. The UV brightenings, in time coincidence with the multiple bursts in hard X-rays, provide evidence (Cheng *et al.* 1984) that the separate bursts represent energy release in different small-scale magnetic structures rather than by repeated flaring of the same loop. Work is now underway to

further our understanding of the link between mass motions seen in soft X-rays and the evaporative process by using *SMM* observations in conjunction with high resolution H α line profile observations obtained at the National Solar Observatory at Sacramento Peak, New Mexico.

In addition to the soft X-ray manifestations of chromospheric evaporation, HXIS observations revealed a sudden coronal explosion toward the end of the impulsive phase (de Jager 1985). This phenomenon is apparently a density wave originating from a small area near, or identical to, the hard

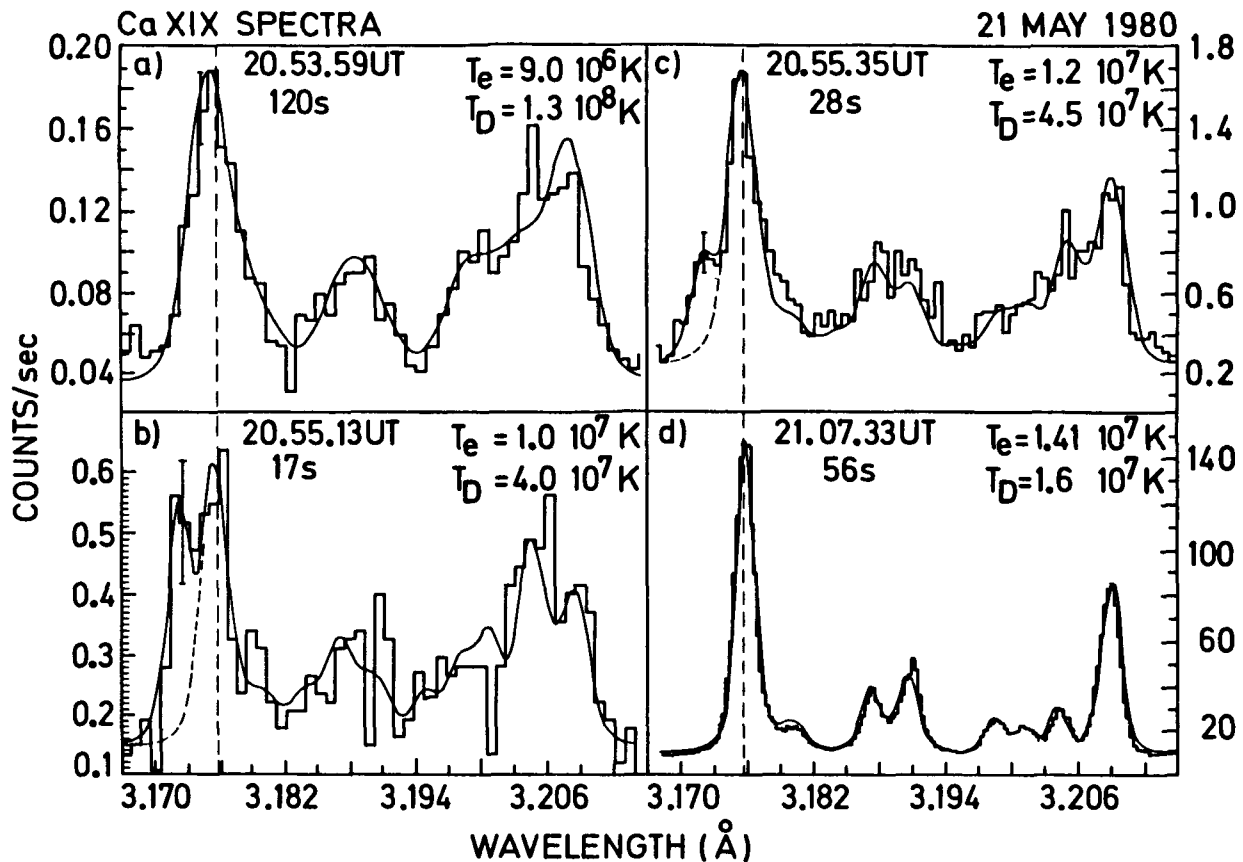


Figure 6. A sequence of soft X-ray Ca XIX (eighteen-times ionized calcium) spectra obtained with BCS during the impulsive phase of a large flare on 21 May, 1980. Note that during the onset of the flare in (a), the line profiles are broadened by mass motions. Later in the impulsive phase (b) and (c), a blue-shifted component can be seen to the left of the peak centered on the broken line at 3.176 Å, indicating an upflow of coronal material at velocities in excess of 200 km s⁻¹. The last frame (d) shows the Ca XIX spectrum at the peak of the gradual phase; no blue shift or line broadening is apparent in this phase of the flare.

X-ray footpoints. The waves propagate with initial velocities of the order of a few hundred to more than a thousand km s⁻¹ which, however, decelerate in only a few minutes to values below 100 km s⁻¹. It has been suggested that the explosion reflects the lateral outstreaming of gas initially convected upwards in the flare footpoints. The upward-moving component of the explosion may accelerate in the progressively less dense plasma above the deceleration region and eventually become a magnetohydrodynamic shock which can produce a propagating (Type II) radio burst high in the corona, as was seen on 21 May 1980 after an X class flare.

While some flares simply cool after the impulsive phase, in others the release of energy continues. In such "dynamic" flares, progressively higher loops become visible in the corona, perhaps through the reconnection of magnetic field lines disrupted early in the flares. HXIS observations show that the loops appear first at the highest energies (22–30 keV),

and only later at lower energies. Since the higher energy channels are much more sensitive to increases in temperature, HXIS observations indicating very small initial sources of this post-flare emission at temperatures $> 50 \times 10^6$ K support the interpretation that successive reconnection of progressively higher field lines continues for several hours (Svestka and Poletto 1985). The loops may extend more than 2×10^5 km above the solar surface, and usually appear to form the most tenuous part of post-flare radio noise storms. These observations are the first direct confirmation of the release of energy long after the initial, impulsive phase of at least some flares. When FCS images of the same events are compared with the HXIS images, it is found that the emission eventually drops toward the solar surface as the emitting plasma cools toward moderate, coronal temperatures. If a new dynamic flare occurs below the large loop structures, they may reappear in 3–30 keV X-rays.

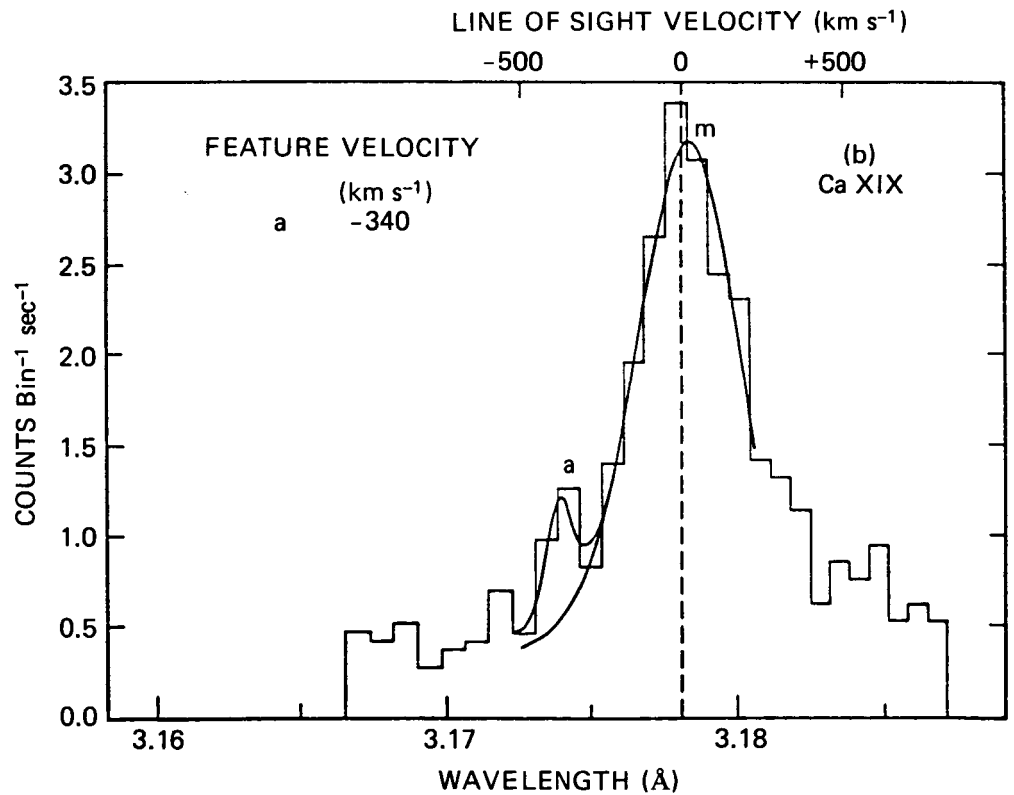
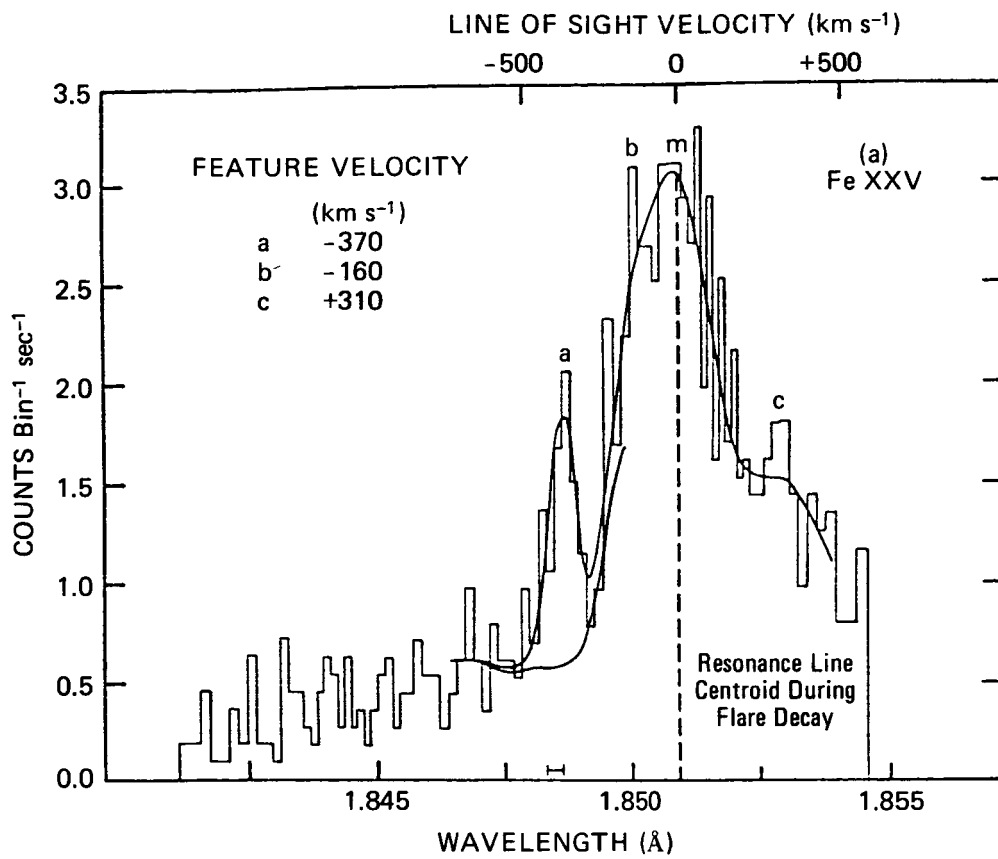


Figure 7. BCS spectra of helium like Fe and Ca resonance lines during the initial phase of a flare on the solar limb on 29 June, 1980. Several features appear on the short-wavelength ("blue") side of the positions of the undisplaced lines, but only feature *a* is considered statistically significant. Its wavelength separation corresponds to an approach velocity ("blue shift") of $\approx 370 \text{ km s}^{-1}$.

ABUNDANCES, SPECTROSCOPY, AND DIAGNOSTICS

Perhaps the most significant advances in instrument design between the *Skylab* and *OSO-8* era and that of *SMM* and *P78-1* have been in the area of high-resolution soft X-ray and γ -ray spectrometers. Resolution of individual line profiles allows us to measure mass flows and nonthermal broadening, and the separation of closely-spaced individual line components permits the use of intensity ratios as diagnostics of plasma temperature and density. The spectrometers on board *SMM* have obtained a variety of significant new observations.

The abundance of the elements is one of the fundamental parameters used in the interpretation of observations of a plasma. Until recently, investigators have been content to adopt a "standard" set of elemental abundances and assume that they remain constant through even extremely dynamic events such as solar flares. Using BCS observations of X-ray flare spectra, however, Sylwester *et al.* (1984) have found startling evidence of variations in the abundance of coronal calcium (Ca). Comparison of spectra obtained in the cooling phases of these flares has demonstrated a variation from flare to flare, and in some cases, there is evidence for changes in the calcium abundance during the heating phase of individual flares. The calcium abundance is determined from the ratio of the intensity of the Ca XIX resonance line (3.173 Å) to that of the nearby continuum. This ratio is a function of the Ca abundance and electron temperature, which can be measured independently from satellite line ratios. A study of over forty flares indicates that the abundance of calcium varies from flare to flare (see Figure 8) by as much as a factor of 2.7.

γ -ray spectra obtained with GRS show many individual lines (Figure 9). These spectra provide unique information on the relative abundance of chemical elements at the γ -ray production site, most probably in the chromosphere. Analysis (Murphy and Ramaty 1985) suggests that the abundances of C and O relative to Mg, Si, and Fe are lower in the chromosphere than in the photosphere. This result also implies a variation of chemical composition with space and time in the solar atmosphere. Since such variations have been observed in solar wind and cosmic ray abundances, and may be reflected in abundances in the winds of other stars similar to the Sun, this discovery may have important implications for our knowledge of cosmic elemental abundances.

These BCS and GRS results may explain some of the discrepancies, often exceeding quoted measurement uncertainties, in solar abundance measurements. More importantly, they raise doubts about

the interpretation of flare data and pose difficult problems for theoretical models of flares, as such models will now have to include a differentiating mechanism to reproduce the changes in the relative abundances of the elements. *SMM* also has the unprecedented opportunity to measure abundances simultaneously in different layers of the solar atmosphere during a flare by using the combined capabilities of GRS and BCS.

Analysis of BCS spectra has concentrated on the numerous dielectronic satellite lines visible to the long-wavelength side of the resonance lines of helium-like and hydrogen-like iron (Fe XXV and Fe XXVI, at ~ 2 Å) and the resonance line of helium-like calcium (Ca XIX, at ~ 3 Å). The ratio of some of these satellites to the resonance line itself is a function of temperature in the case of satellites due to the lithium-like stage, while for satellites due to lower stages there is also a density dependence. The theory and comparison with BCS and other observations of the density-dependent satellites are given in papers by Phillips *et al.* (1983) and Lemen *et al.* (1984, 1986). These papers deal not only with iron spectra from the Sun, but also with spectra due to other metals which should soon be available from tokamaks and other fusion devices. Comparison of theoretical iron spectra for the stages Fe XIX - XXIV with BCS flare spectra (Figure 10) shows excellent agreement; the density-dependent stages Fe XIX - XXI reveal an upper limit to the electron density of 10^{12} cm $^{-3}$.

In an extensive spectral scan with the FCS during a class SB flare on 25 August, 1980, some 205 lines were distinguished, and Phillippe *et al.* (1982) were able to identify all but 40 of them. Several lines were seen for the first time, and the whole of the 5 - 19 Å region was seen with a spectral resolution that is still unsurpassed. The region near the helium-like neon lines at 13.5 Å was of particular interest in this respect, as previous instruments had not resolved the neon lines from the numerous Fe XIX lines. With the beryl crystal of channel 2 of the FCS, the various line blends are much better resolved, though an analysis of the neon lines (Wolfson *et al.* 1983) for electron density may still require correction for remaining Fe XIX line blends. Some lines due to Fe XXI and Fe XXII, 2-3 transitions, are visible at ~ 12 Å. Lines due to transitions from the ground state of these ions are visible, but those from excited states are not (see Figure 11), giving an upper limit to the electron density for this flare of $\sim 10^{12}$ cm $^{-3}$, in agreement with the BCS results.

An exciting new data set - a long FCS spectral scan during an M4 flare on 2 July, 1985 - has resulted in several new line identifications and new

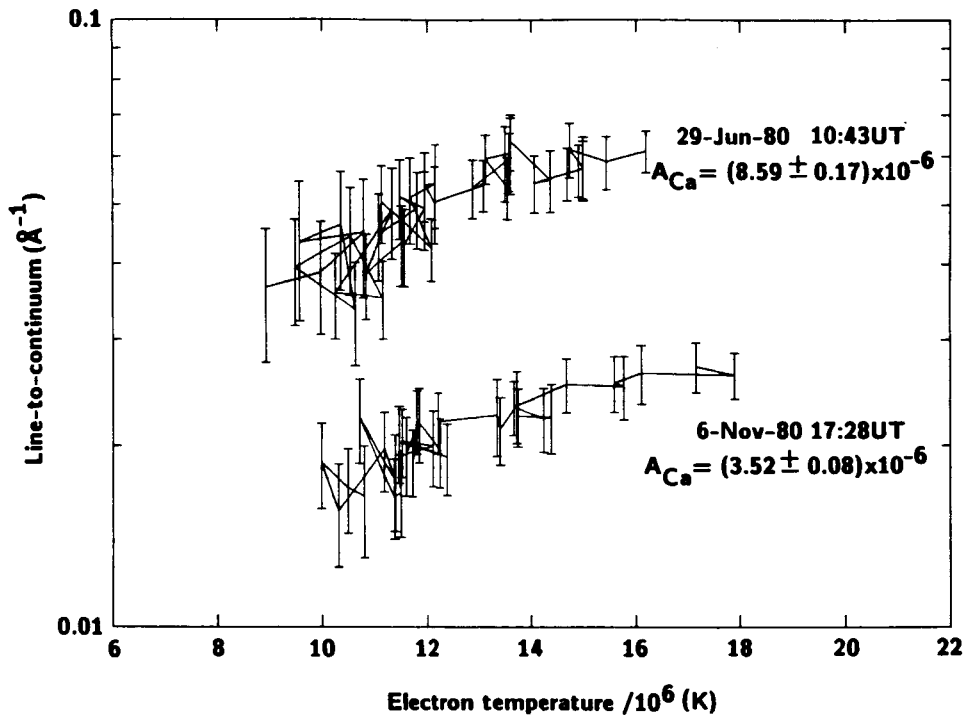


Figure 8. The ratio of the soft X-ray Ca XIX resonance line intensity to the nearby continuum, as observed by BCS during the cooling phase of two flares with different coronal calcium abundances A_{Ca} . (The intensity ratio depends only weakly on temperature.) The curves are normalized in such a way that the values are proportional to A_{Ca} , and the error bars are $\pm 1\sigma$ uncertainties determined by the line-fitting procedures.

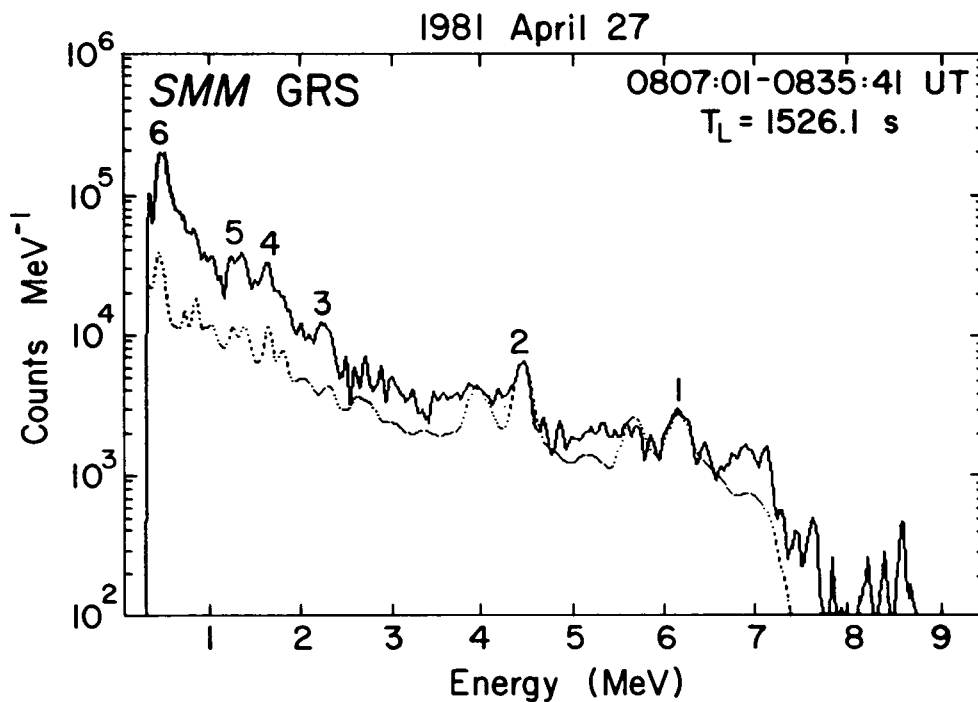


Figure 9. A γ -ray flare spectrum obtained by GRS (solid line) and a fit to it (dashed line) based on relative elemental abundances that differ from standard solar values. In particular, the abundances of C and O are lower, relative to those of Mg, Si, and Fe.

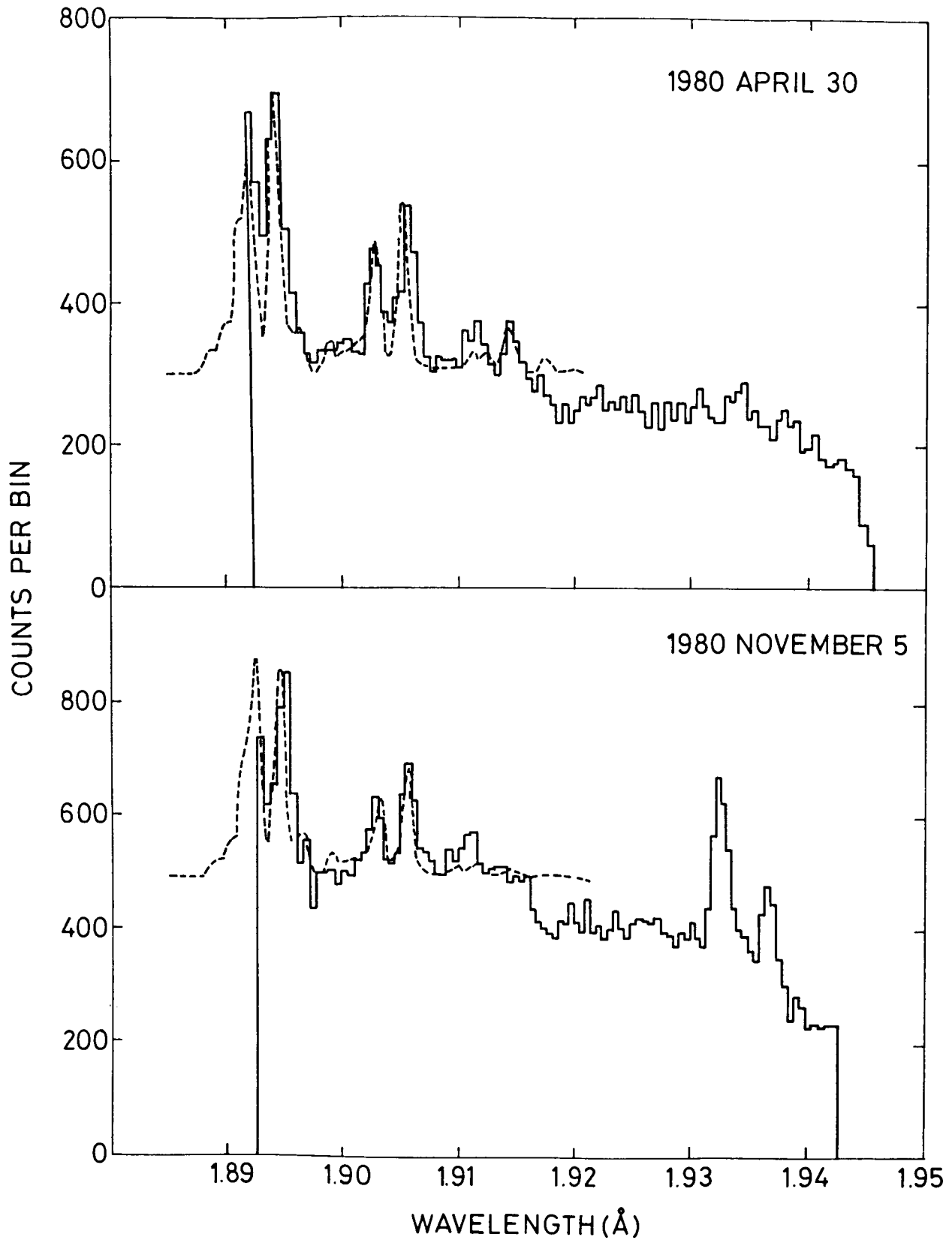


Figure 10. BCS spectra (histograms) near the peaks of two flares, compared with theoretical spectra (dashed lines) calculated in the low density limit ($n_e < 10^{12} \text{ cm}^{-3}$). The line features at 1.89 Å are due to Fe XXI; at 1.90 Å, to Fe XX; and at 1.91 Å, to Fe XIX. The two lines at 1.93 - 1.94 Å are the $K\alpha$ lines from neutral or near-neutral Fe.

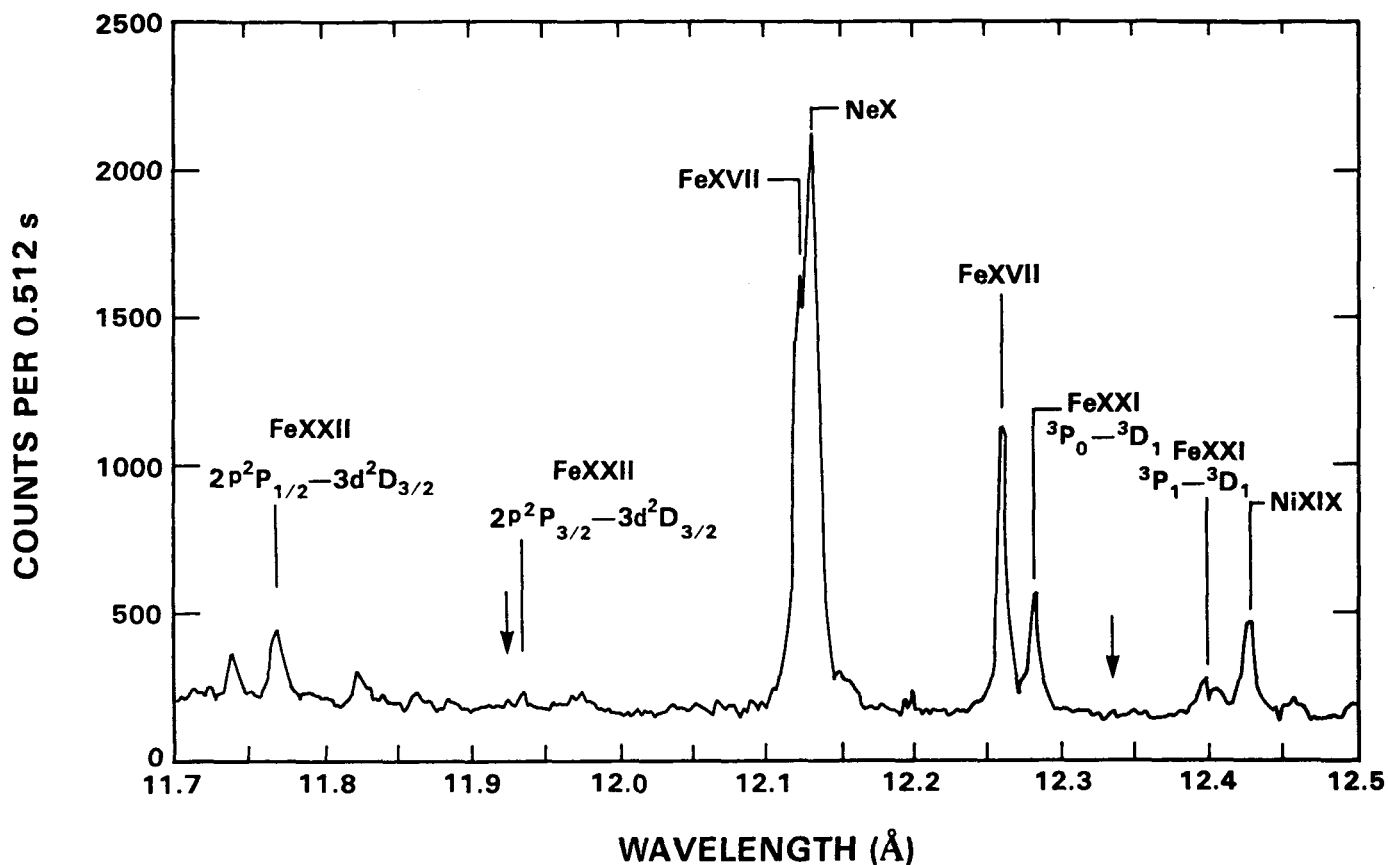


Figure 11. FCS spectrum of the 12 Å spectral region during the SB flare of 25 August, 1980. In addition to the positions of known Fe XXI and Fe XXII lines, the locations of lines of these ions at densities of greater than 10^{12} cm^{-3} are marked with arrows.

density diagnostics (Fawcett *et al.* 1987). The lines occur between 8 and 10 Å, covered by FCS channel 3. Comparison with laboratory and theoretical wavelengths shows that most of the lines are due to $n = 2 - 4$ transitions of Fe XX - XXII. Although complete atomic theory is lacking, the Fe XXII lines can be analyzed for electron density, which is found to be $> 10^{12} \text{ cm}^{-3}$. There should be similar density-dependent lines of Fe XX and Fe XXI. Two long-standing spectral identification puzzles are solved by this work: the lines at 17.62 and 18.97 Å, seen previously in several FCS channels 1 spectra, are in fact second-order Fe XXII and Fe XXI lines arising from $n = 2 - 4$ transitions.

ENERGETICS

A critical test of our understanding of the flare mechanism lies in our understanding of the evolution of the energy budget - the net sources and sinks of flare energy - throughout the flare. The solution

of this difficult problem requires knowledge of the major physical mechanisms that govern the storage, release, transport, and dissipation of the energy released during a flare. One of the strengths of the *SMM* observatory is the ability to make the coordinated multiwavelength observations needed for progress in the understanding of flare energetics. BCS spectral observations of chromospheric evaporation have provided the first measurements of the kinetic energy of the mass motions in the coronal plasma during a variety of flares (Antonucci *et al.* 1984). In some flares, this component of the energy budget is comparable both to the energy released in the impulsive phase in the form of electron beams, and also to the thermal energy measured at the peak of the gradual phase of the flare (Wu *et al.* 1986).

A study of the energy budget of multiple flares (see Figure 12) led to the discovery (Strong *et al.* 1984) that the distribution of the released energy into its various forms is critically dependent on the preflare conditions in the corona.

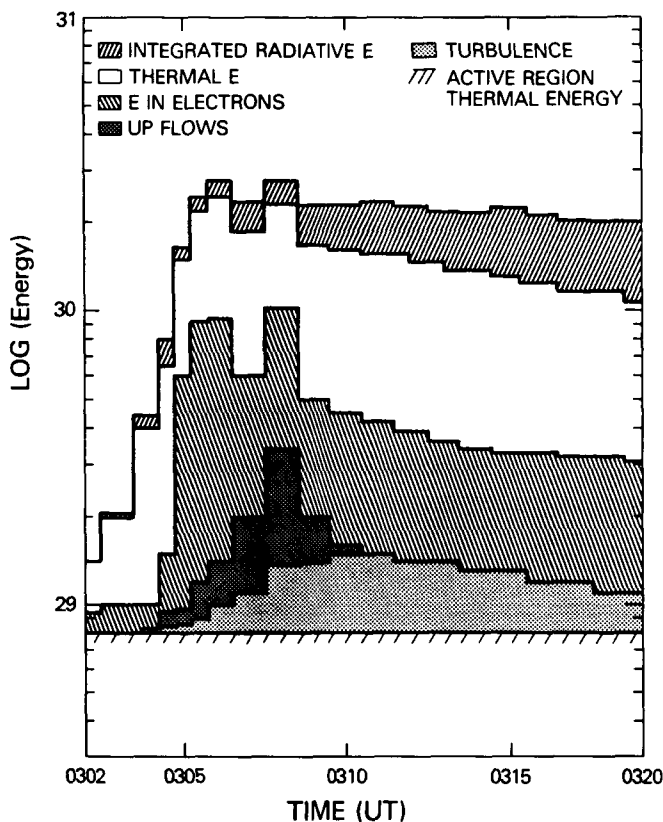


Figure 12. The distribution of flare energy among various reservoirs and active phenomena as a function of time during the 8 April, 1980 flare. The width of the histogram bins represents the temporal resolution for each parameter displayed. Note that after the peak at about 03:06 UT, the sum of the various components remains effectively constant, even though the individual components are varying.

References

Antonucci, E. and Dennis, B. R. 1983, *Solar Physics*, 86, 67

Antonucci, E., Gabriel, A. H., and Dennis, B. R. 1984, *The Astrophysical Journal*, 287, 917

Bentley, R. D., Lemen, J. R., Phillips, K. J. H., and Culhane, J. L. 1986, *Astronomy and Astrophysics*, 154, 255

Cheng, C.-C., Tandberg-Hanssen, E., and Orwig, L. E. 1984, *The Astrophysical Journal*, 278, 853

Chupp, E. L. 1984, *Annual Reviews of Astronomy and Astrophysics*, 22, 359

Chupp, E. L. *et al.* 1982, *The Astrophysical Journal*, 263, L95

de Jager, C. 1985, *Solar Physics*, 96, 143

Doschek, G. A., Kreplin, R. W., and Feldman, U. 1979, *The Astrophysical Journal*, 233, L157

Duijveman, A., Hoyng, P., and Machado, M. 1982, *Solar Physics*, 81, 137

Fawcett, B. C., Jordan, C., Lemen, J. R., Phillips, K. J. H., 1987, to be published in *Monthly Notices of the Royal Astronomical Society*

Forrest, D. J. and Chupp, E. L. 1983, *Nature*, 305, 291

Gunckler, T. A., Canfield, R. A., Acton, L. W., and Kiplinger, A. L. 1984, *The Astrophysical Journal*, 285, 835

Hoyng, P., *et al.* 1981, *The Astrophysical Journal*, 246, L155

Kiplinger, A. L., Dennis, B. R., Emslie, A. G., Frost, K. J., and Orwig, L. E. 1983, *The Astrophysical Journal*, 265, L99

Lemen, J. R., Phillips, K. J. H., Cowan, R. D., Hata, J., and Grant, I. P. 1984, *Astronomy and Astrophysics*, 135, 313

Lemen, J. R., Phillips, K. J. H., Doschek, G. A., and Cowan, R. D. 1986, submitted to *Journal of Applied Physics*

Murphy, R. J. and Ramaty, R. 1985, *Advances in Space Research*, 4, 127

Phillips, K. J. H. *et al.* 1982, *The Astrophysical Journal*, 256, 774

Phillips, K. J. H., Lemen, J. R., Cowan, R. D., Doschek, G. A., and Leibacher, J. W. 1983, *The Astrophysical Journal*, 265, 1120

Strong, K. T. *et al.* 1984, *Solar Physics*, 91, 325

Svestka, Z. and Poletto, G. 1985, *Solar Physics*, 97, 113

Sylwester, J., Lemen, J. R., and Mewe, R. 1984, *Nature*, 310, 665

Vestrand, W. T., Forrest, D. J., Chupp, E. L., Rieger, E., and Share, G. 1986, submitted to *The Astrophysical Journal*

Woodgate, B. E., Shine, R. A., Poland, A. I., and Orwig, L. E. 1983, *The Astrophysical Journal*, 265, 530

Wolfson, C. J., Doyle, J. G., Leibacher, J. W., and Phillips, K. J. H. 1983, *The Astrophysical Journal*, 269, 319

Yoshimori, M., Hirasima, Y., and Okudaira, K. 1983, *Solar Physics*, 86, 375

Wu, S. T. *et al.* 1986, in *Energetic Phenomena on the Sun: Proceedings of the SMM Workshop*, eds. Woodgate, B. E. and Kundu, M. R. (NASA CP-NN, Washington, D.C.), chap. 5

THE ACTIVE SOLAR ATMOSPHERE

Although flares represent the most intense energy dissipation of any form of solar activity, the active Sun has many other manifestations. These include sunspots, photospheric faculae, chromospheric and transition region plages (probably made up of small loop structures), large coronal loops, and even larger scale coronal streamers and occasional coronal mass ejections. In addition, prominences (referred to as filaments when seen in H α absorption on the disk), while a quiet solar phenomenon as well, frequently form over the neutral line separating areas of an active region with opposite magnetic polarities. All of these phenomena are dynamic, on time scales ranging from seconds to the complete solar magnetic cycle of 22 years. *SMM* instruments, with high temporal, spatial, and spectral resolution, have been able to provide new insights into a variety of these phenomena. The extended lifetime of the *SMM* mission in turn has allowed unprecedented diachronic observations of some of the global properties of the coronal magnetic field.

CORONAL MASS EJECTIONS: STRUCTURE AND FREQUENCY

A major goal of the *SMM* Coronagraph/Polarimeter (C/P) has been the study of the detailed properties of a class of solar activity called coronal mass ejections, or coronal transients. These ejections were discovered in the early 1970's and were the subject of intensive investigation based on results from the *Skylab* coronagraph. They involve the ejection of millions of tons of coronal material from the lower solar atmosphere, in concert with solar flares and/or eruptive prominences. It has been conjectured that coronal mass ejections cause geomagnetic activity when their path through the interplanetary medium intersects the magnetic fields in the environs of the earth. Although the physical mechanism responsible for such ejections is still a matter of active study, the results from the *SMM* have proven to be extraordinarily valuable in examining the properties of coronal mass ejections, both in regard to their general characteristics and in studying the detailed aspects of specific events. In turn, these studies are leading theoretical astrophysicists toward an understanding of the physical mechanisms which govern these phenomena.

The ability of C/P to image with high spatial resolution ($\leq 10''$) and to provide images of extraordinary clarity has elucidated the origin and nature of

the main components of mass ejections. The principal features of a typical loop-like mass ejection (now known to make up a majority of all such events) are the presence of a bright, "frontal" loop, followed by a dark cavity, within which is often visible a bright structure. These elements are now identified with, respectively, pre-existing inner coronal magnetic loops, the prominence-coronal cavity, and prominence material itself (Figure 13). Observations obtained with the C/P and ground-based coronameters able to observe the lower solar corona suggest that loop-like mass ejections form when the cavity beneath a coronal helmet streamer containing a prominence rises from an equilibrium state. The intrusion of this cavity, probably a region of strong magnetic field, into the corona deforms the helmet streamer into the bright, frontal loop.

Prior to the 1980 *SMM* period, it had been conjectured that the overall frequency of coronal mass ejections might follow the rate of occurrence of sunspots on the Sun - that is, transient frequency would be proportional to the general level of activity. While the C/P results indicate a general variation of CME frequency with solar activity, it is difficult to see any close relationship between that frequency and measured sunspot number. Figure 14 shows the rate of occurrence of mass ejections (per day) inferred from *Skylab* (1973-1974) and C/P (1980, April, 1984 - December, 1985) observations. The error bars indicate the range of uncertainties introduced by various assumptions in estimating the duty cycle of the observations. The CME rate increased only slightly between the *Skylab* and the first *SMM* (1980) periods; given the large duty cycle corrections and potential problems with the threshold for counting transient events observed by different instruments, it is possible that there was no change. Between the first (1980) and second (1984-1985) *SMM* epochs, however, the CME frequency dropped significantly. The small duty cycle corrections for the second *SMM* period make this conclusion certain. It is still impossible, however, to fit all of these rates with a simple relationship to sunspot number. In particular, the *Skylab* and 1984 *SMM* observations were made at phases of the cycle when the sunspot numbers were virtually identical, but the best estimates of CME frequency for these times vary by a factor of ~ 3 .

A similar situation arises on examination of the speeds of coronal mass ejections. Most of the events detected in 1984 and 1985 were moving at lower speeds than those from the *Skylab* and 1980 *SMM*



Figure 13. A coronal mass ejection (CME) in progress, as seen in C/P images. This event, which occurred on 14 April, 1980, illustrates the principal features of many CME's: the presence of a bright, outer loop of material, followed by a dark cavity, under which is visible a bright loop-like structure identified with erupting prominence material. The time sequence covers almost 3 hours (from 04:40 UT to 07:09 UT on 14 April, 1980). The outward movement of the ejection is clearly evident; the outer loop is moving outward from the Sun at about 270 km s^{-1} .

epochs. This change can be seen in Figure 15, which shows the averages and medians of all CME speeds measured in those periods. By either of these statistical parameters, the typical speed of mass ejections decreased by a factor of ~ 3 from 1980 to 1984-1985. Any attempt to correlate this variation

with sunspot number, however, must be tempered on examination of the *Skylab* measurements from 1973-1974. Despite the low level of solar activity in 1973-1974, more high-speed mass ejections were observed at that time than during any of the times for which *SMM* observations are available, including

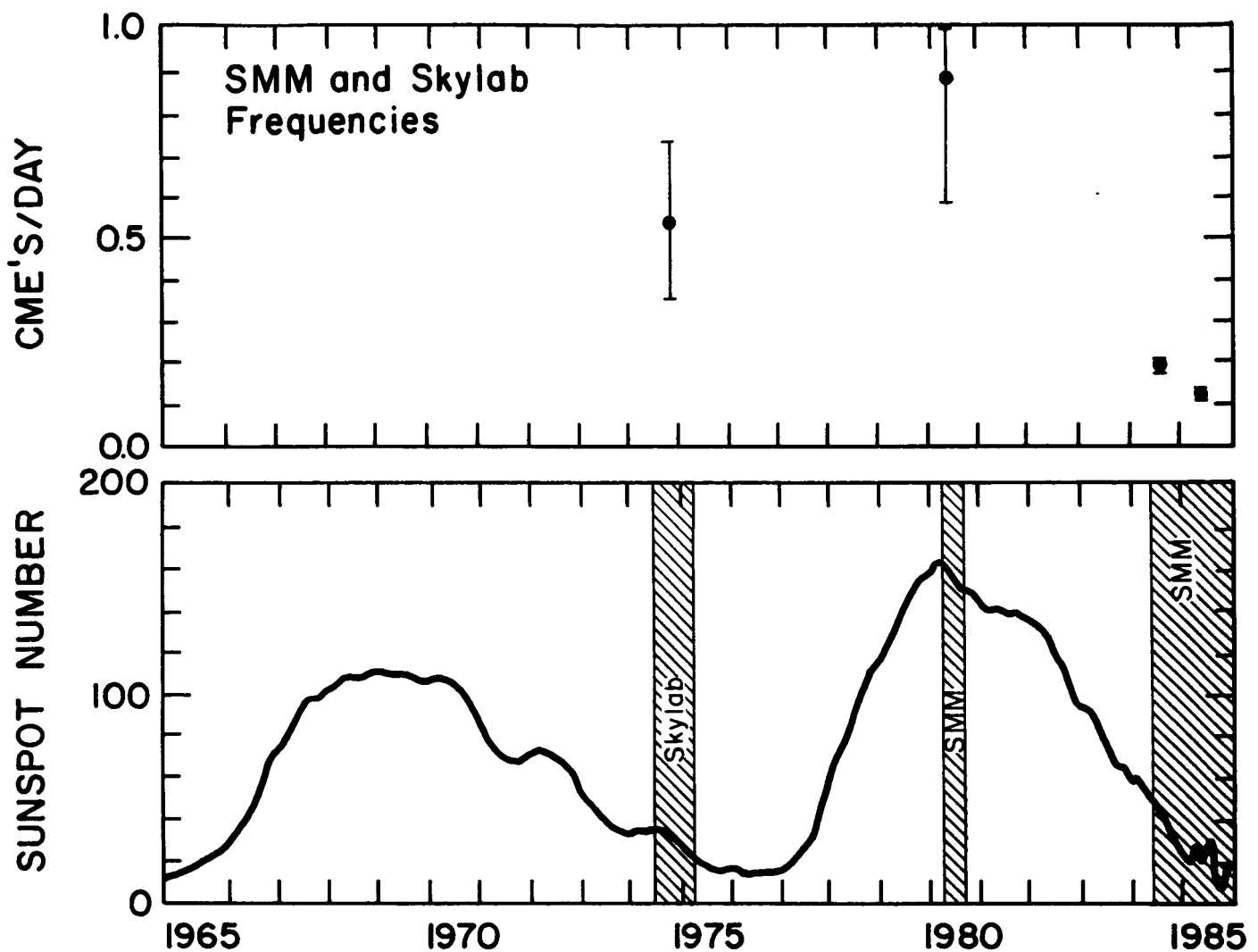


Figure 14. The frequency of coronal mass ejections (top) and sunspot number (bottom) during the last two solar cycles. The periods when *Skylab* and *SMM* coronagraphs were operating are shown in the lower panel as hatched areas. The *SMM* Coronagraph/Polarimeter is still in operation.

the maximum of solar activity in 1980. The apparent solar latitude of coronal mass ejections, however, does appear to change systematically with the phase of the solar cycle. Like the rays, helmet streamers, and other bright features in the "quiet" corona, the mass ejections tend to occur near the solar equator around sunspot minimum (1984-1986) and spread over a wide range of latitudes at maximum (1980). This change will tend to mitigate any temporal variations in the interplanetary effects of coronal mass ejections seen in the ecliptic plane.

CORONAL MASS EJECTIONS: ORIGIN AND ENERGETICS

Since the inner edge of the C/P field of view is limited to ≥ 0.5 solar radii above the photosphere

by light scattered around the coronagraph's occulting disk, combination of C/P data with that of X-ray, ultraviolet, and ground-based $H\alpha$ instruments is crucial to understanding the origin of coronal mass ejections. One important new suggestion for the solar surface association of coronal mass ejection events has arisen from a detailed comparison of results from C/P and HXIS. It is natural to associate the expulsion of material with the energy release in a flare. After all, we expect that following the explosion the secondary products will expand outward rapidly. Careful extrapolation of the altitude-time history of a number of transients, however, led to a suggestion that the mass ejections might actually leave the Sun before the optical flare with which they were associated. Confirmation of this fact is clearly very important, for if the mass ejections precede the flare, then perhaps the flare itself is a

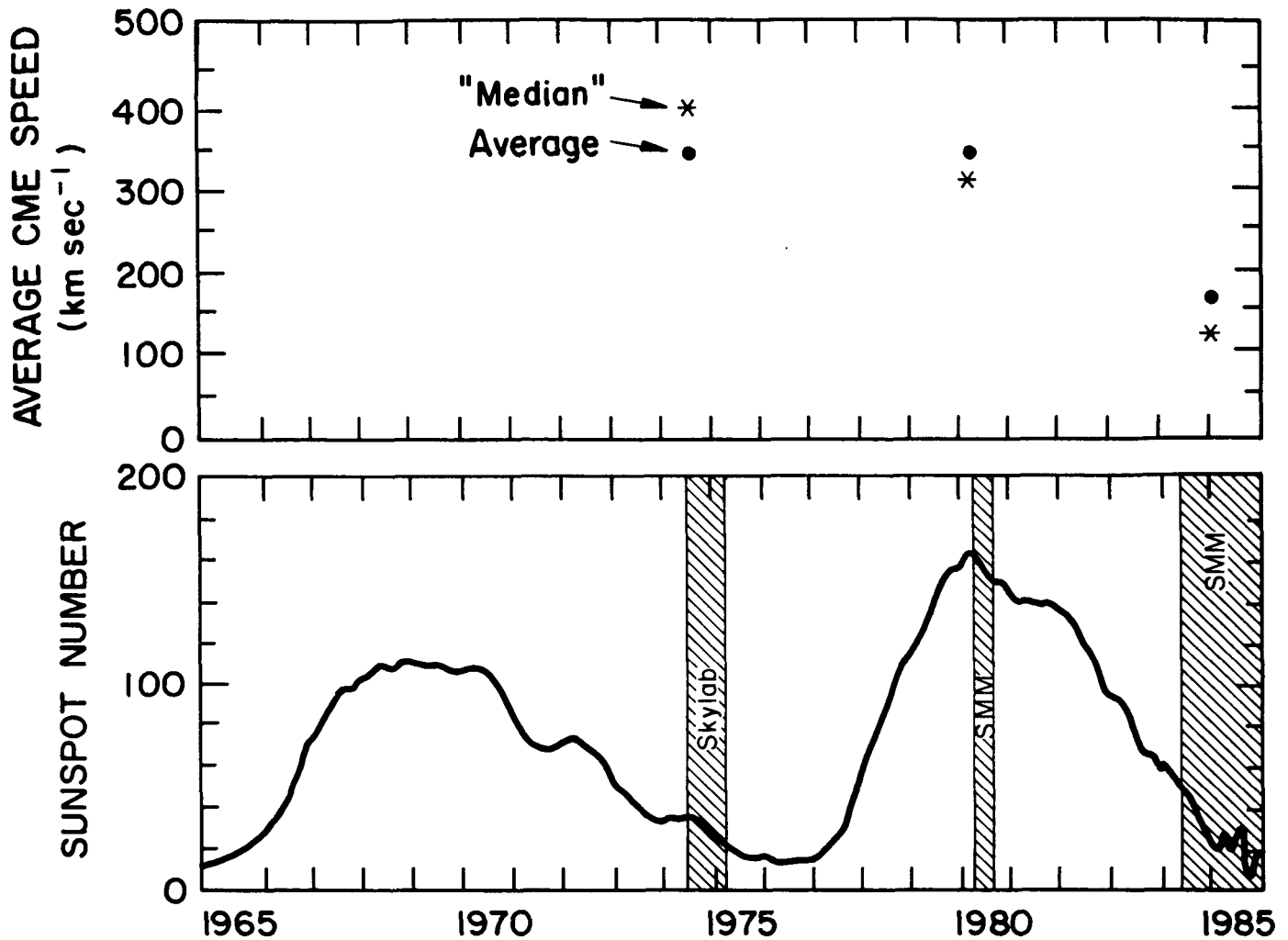


Figure 15. Average and median speeds of coronal mass ejections observed by the *Skylab* White Light Coronagraph and *SMM* C/P (top), and corresponding sunspot number measurements (bottom). Note the differences in speeds for the two periods of near-minimal solar activity (1974 and 1985).

consequence of the ejection, rather than a direct cause. It has been known for some time that the kinetic energy of mass ejections is considerably greater than estimates of the radiated energy of any associated flare, but the relation between the ejection and the flare itself remains unclear.

Evidence for preflare origin of ejections was obtained from HXIS data by Simnett and Harrison (1985), who discovered a very small soft X-ray (3.5–5.5 keV only) enhancement some 15–20 m before the main optical flare. An example is shown in Figure 16(a) for the limb event on 29 June, 1980 at 02:33 UT. A small soft X-ray precursor at 02:12 UT (left panel) is followed by a class M3 flare (shown with very different intensity scaling in the right panel.) Superposed on these plots are the altitude-time histories of the white-light coronal mass ejection (crosses) observed by C/P and an X-ray transient (horizontal lines marked a, b, c), which are referred

to the scale on the right of Figure 16(a). The dotted line is a projection backward in time of the best-fit straight line through the crosses. The mass ejection must undergo some acceleration in its initial phase, which would cause the extrapolation to bend towards earlier times. Therefore, a reasonable altitude-time plot would link the intervals a, b, c with the crosses in a smooth, continuous line. In this interpretation, then, the initiation of the transient would be 02:12 UT rather than at the onset of the main optical flare at 02:35 UT.

The HXIS images also suggest the presence of widely separated footpoints of the loops revealed in the C/P images. Figure 16(b) shows the 3.5–5.5 keV image for the period covering the precursor. Two centers of activity are seen on the limb, separated by over 75,000 km; the main flare came from region A. Examination of X-ray images prior to other transients shows that the simultaneous

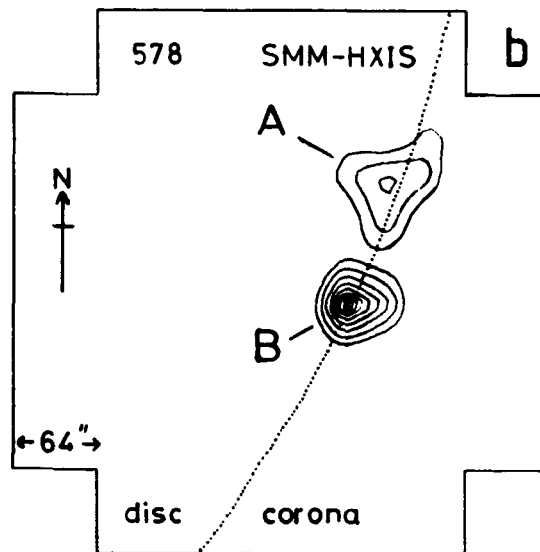
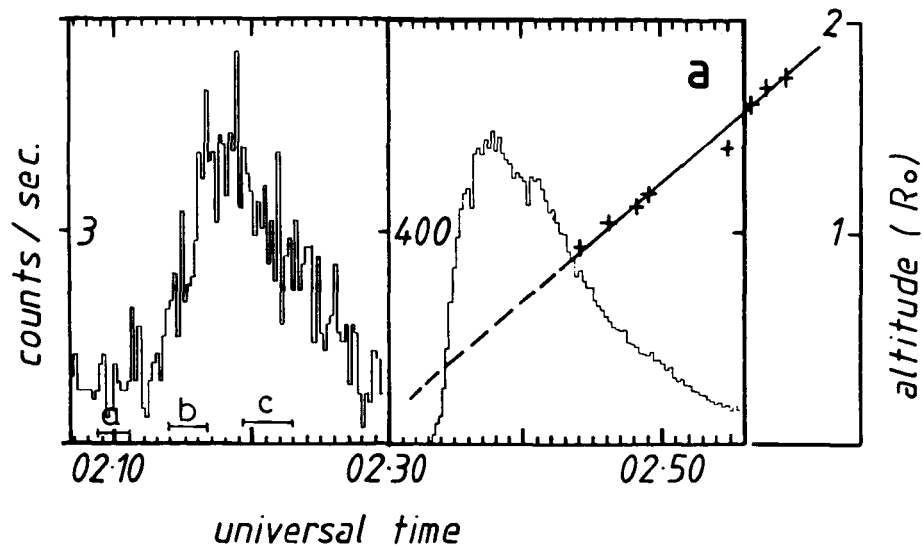


Figure 16. HXIS observations of a coronal mass ejection: (a) 3.5 - 5.5 keV intensity time profile for the flare at 02:33 UT on 29 June 1980, and its precursor (note the scale change at 02:30 UT). Superposed onto this are the altitude histories of the white-light coronal mass ejection (crosses) and, during the precursor, an X-ray transient (horizontal bars a, b, c). (b) the 3.5 - 5.5 keV image for the period covering the precursor.

activity from widely separated points is not unusual. Apparently, then, the remote sites represent foot-points of a large coronal structure which contains the mass ejected in the transient. Energy release within this large structure, presumably through interacting magnetic fields, leads to the acceleration of non-thermal, charged particles. Some of these are guided to the footpoints of the magnetic loop where they heat the coronal/chromospheric plasma to $6-7 \times 10^6$ K to produce the soft X-ray enhancement. At the same time, energy losses in the high corona destabilize the structure and initiate the transient.

Subsequent evolution of the magnetic fields as a result of this activity not only produces more energy release, to power the main optical flare, but also drives the mass outwards against solar gravity.

It appears, then, that the initiation of coronal mass ejections is best associated (both spatially and temporally) with the occurrence of small X-ray "microbursts," as opposed to larger, more conventional flaring regions. This new association has been found for more than a half-dozen events for which simultaneous coronagraph and HXIS data are available, and a search continues for more examples,

both in the HXIS and C/P archival databases, and in new FCS and C/P data. If this new association is found to be typical, it will provide important new boundary conditions for the energy input to the mass ejection. Specifically, it would then be less likely that a pressure pulse (driven by a density enhancement or a temperature enhancement, or both) of extended duration at the base of the corona drives coronal mass ejections. Instead, the two most likely driving mechanisms for coronal transients would then be magnetically-driven and pressure-driven events. Since the highly ionized coronal plasma is so tenuous that any mass motions in it are directed by the magnetic field, a disruption of the field rising from the lower solar atmosphere, would carry along the visible plasma. In the case of a pressure-driven event, the driving would originate in the explosive release of energy at the base of the atmosphere. Such an explosion could be the result of either a sudden liberation of thermal energy or a sudden density increase. A major task confronting theoretical astrophysicists, then, is the determination of the correct driving force involved in coronal mass ejections.

Theoretical ideas involving the pressure-driven model for coronal mass ejections continue to be refined and improved. Stimulated by a detailed quantitative comparison between earlier models of this type and the properties of the most general class of mass ejections, additional efforts have been devoted toward improving the models so that their predictions are in closer agreement with the observations. As noted above, the basic tenet of the wave models is that the transient occurs as a result of the deposition of energy within a localized region in a given coronal atmosphere. After specifying the initial coronal conditions and details of the energy input, the time-dependent magnetohydrodynamic equations are solved numerically to simulate the resulting transient. The energy source is generally assumed to be either thermal or kinetic as far as the model is concerned, although it may occur as a result of small-scale processes not included in the global (large-scale) representation.

Early models employing a static atmosphere with an embedded force-free magnetic field as the medium through which the transient propagates, could not reproduce any of the principal features of mass ejections. Recently, however, an improved model (Steinolfson 1987) in which the energy release occurs at the base of a preexisting simulated coronal streamer has better approximated a number of the principal features of observed coronal mass ejections. A major problem remained, however: that of properly simulating the appearance of the top of the leading-edge transient loop, which always

appears dimmer in reality than in simulation. This problem has recently been qualitatively resolved with the inclusion of a radially dependent heating term, selected to maintain a prescribed temperature distribution in the atmosphere. At present, therefore, it appears that such models can simulate many of the principal features of real coronal mass ejections.

GLOBAL PROPERTIES OF THE CORONAL MAGNETIC FIELD

The global properties of the corona reveal the state of the global solar magnetic field. It has long been recognized that this magnetic field assumes a particularly simple form near periods when the sunspot number is low, the time of solar minimum. At that time, the global magnetic field is appropriately described as a dipolar field, not unlike that produced by a bar magnet whose magnetic poles are aligned with the solar rotational poles. In recent years, this simple picture has been modified to include the fact that the magnetic poles are, in fact, tilted with respect to the rotation axis. The degree of tilt is a function of the time in the solar cycle. Measuring the change in the tilt angle of the magnetic axis provides a measure of the rate of change of the evolution of the global magnetic field and hence of the internal dynamo driving the system. The measurements can be made from coronagraph images, where the center of brightness of coronal features is identified with the global "neutral sheet" (the plane which separates the two magnetic polarities). Interestingly, the rate of change of the tilt angle in 1984-1985 is on the order of $0.1^\circ \text{ day}^{-1}$, about twice as rapid as in the comparable period of the previous solar cycle (Figure 17), and while in mid-1984, the neutral sheet was inclined by $\sim 30^\circ$ to the plane of solar equator, by early 1986, the tilt decreased to 5° to 10° .

Finally, the global structure of the coronal magnetic field can be revealed from coronagraph observations with the use of so-called "synoptic maps," analogous to the familiar Mercator cylindrical projection used in many maps of the Earth. The solar counterpart displays the brightness of the corona on a plot of solar latitude and longitude. The degree with which the map changes with time is a measure of the variability of the solar corona (Figures 18 and 19). Especially striking is the difference between synoptic maps constructed from results gathered over the 1980 *SMM* period, near solar maximum, and those from 1985, not long before solar minimum. Such displays vividly point out the ordered, regular structure present at periods of low solar

ORIGINAL PAGE
COLOR PHOTOGRAPH

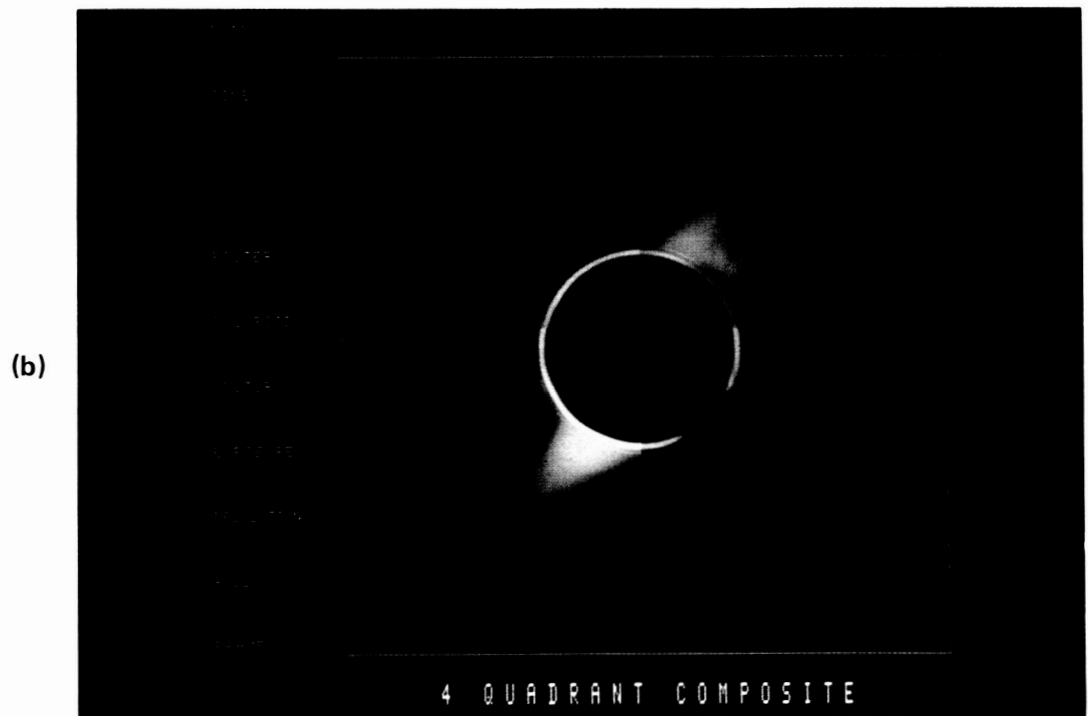


Figure 17. The superposition of four images from different sectors or "quadrants" to show the corona around the entire Sun in (a) 1980 and (b) 1985. The 1980 composite shows a typical sunspot maximum corona - bright streamers and rays appear at virtually all solar latitudes and there are no conspicuous polar coronal holes. In contrast, the 1985 image shows a corona more typical of conditions just before sunspot minimum. Bright helmet streamers and rays are confined to low solar latitudes and there are conspicuous polar coronal holes. However, the corona is not symmetric about the solar rotation axis (as in all the *SMM* coronagraph images, this axis runs diagonally across the image, from upper left to lower right), but about an axis inclined about 20° from that of rotation. The corona thus resembles the "tilted dipole" seen in 1974-1975, just before the previous sunspot minimum.

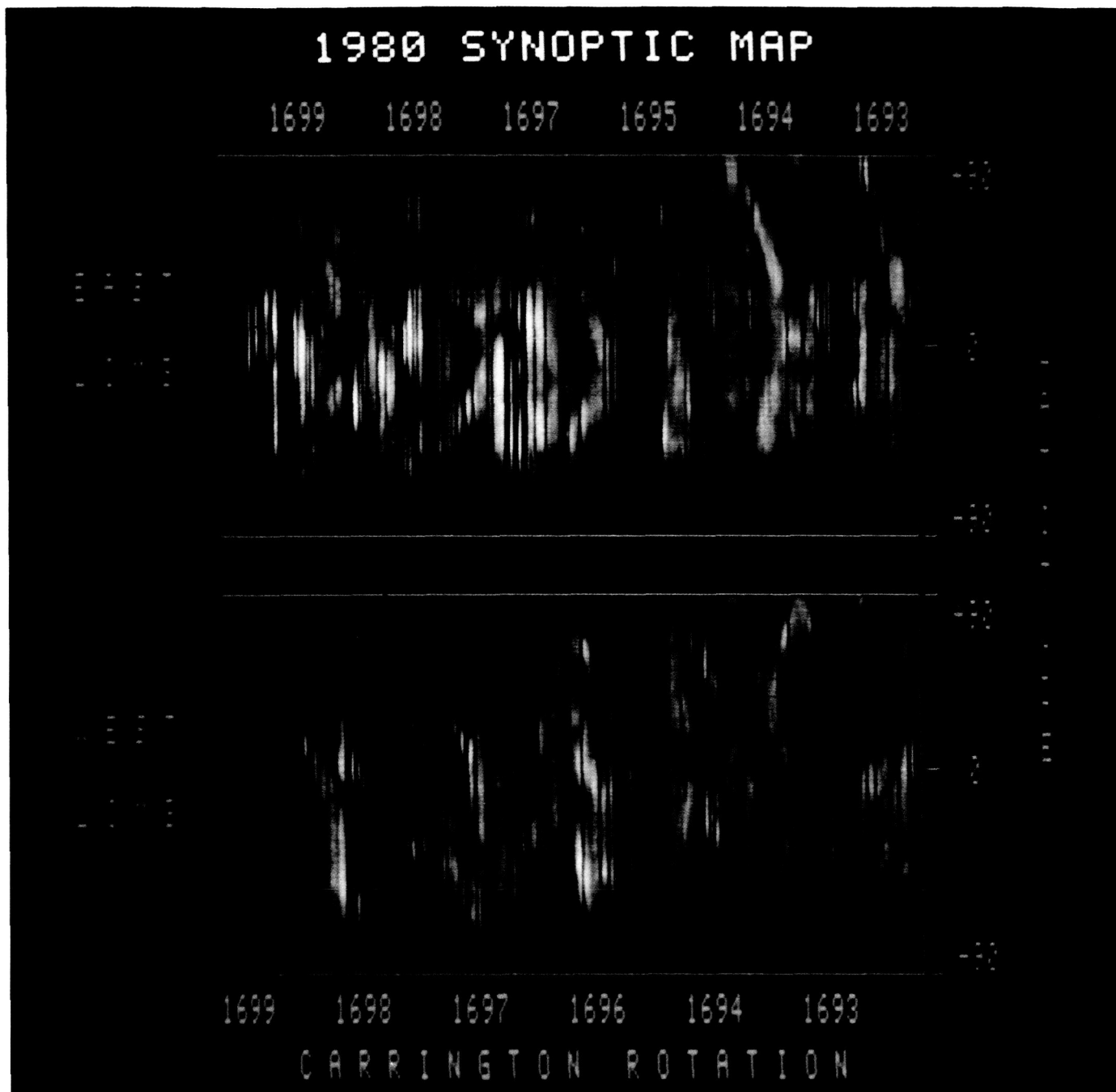


Figure 18. A synoptic map constructed from 1980 *SMM* coronagraph data. Observations from the east and west solar "limbs" have been used to generate separate maps of coronal brightness vs. solar latitude and Carrington longitude (of the limb at the time of observation) for Carrington Rotations 1693-1699. The dark, vertical stripes are data gaps of 12 hours or more. This 1980 map shows the absence of polar holes, the presence of many bright features at all latitudes, and little tendency for features to persist for many rotations of the Sun. All of these properties are characteristic of the sunspot maximum epoch.

activity, in contrast to the more chaotic, irregular structures present near periods of maximum activity (Hundhausen 1987). These maps permit investigations of the scale of structures, their longevity, and their interrelationships with other solar parameters.

ACTIVE REGION HEATING

Possibly one of the most surprising results to come from the FCS data was the observation by Acton *et al.* (1981) of significant non-thermal broadening of the lower-temperature ($2-5 \times 10^6$ K)

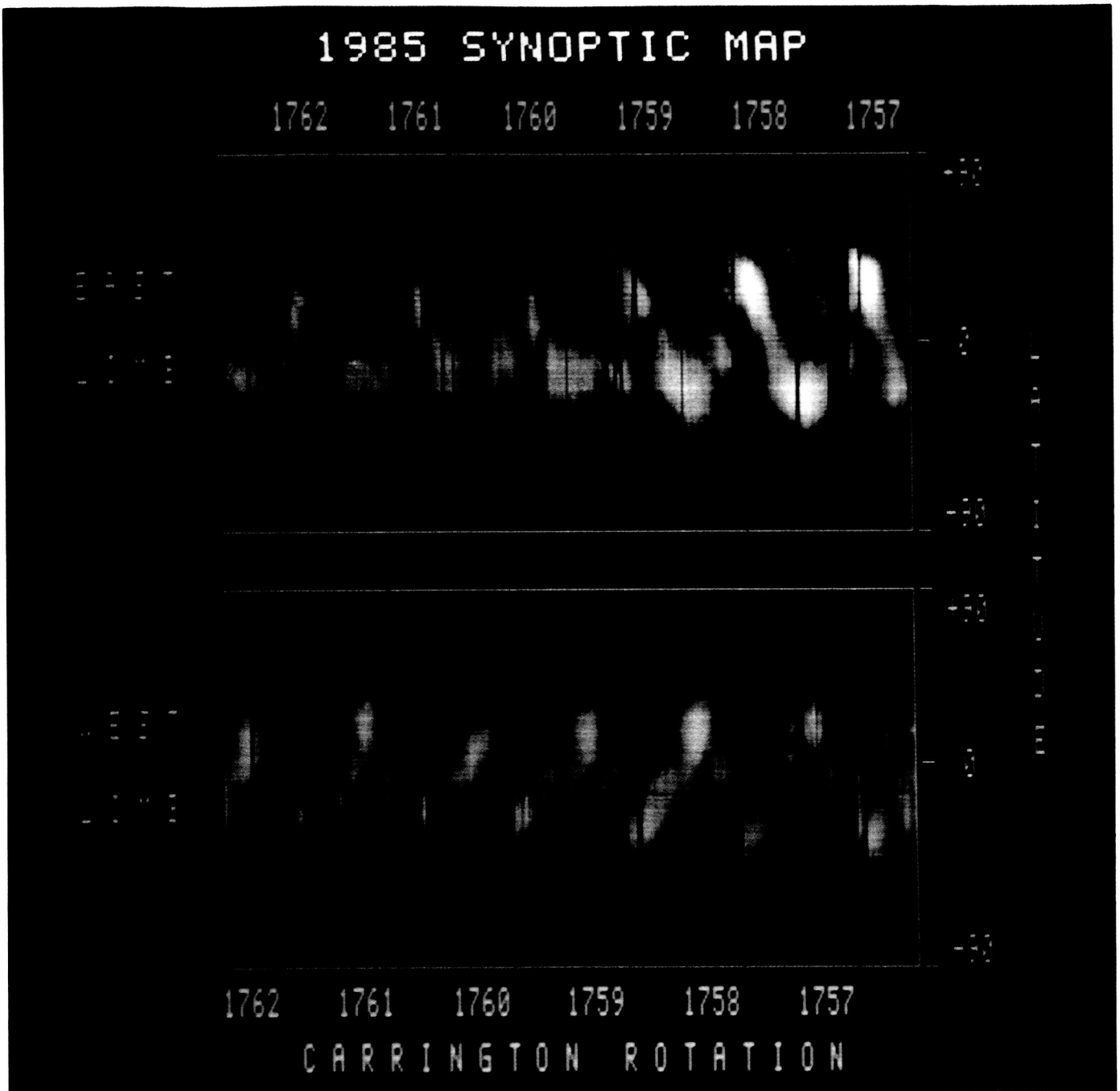


Figure 19. Synoptic map generated from 1985 *SMM* coronagraph data. In contrast to Figure 18, this map shows conspicuous polar holes, and each polar hole extends a significant distance toward the solar equator, with about 180° difference in the Carrington longitudes of the extensions. Considerable persistence of features for many solar rotations are also visible. The sine wave-like belts of bright corona separating the two polar holes and their equatorward extensions again suggests a tilted dipole corona similar to that seen in 1974–1975. The slow “squeezing” of this belt toward the equator implies a gradual decrease of the “tilt angle” as sunspot minimum approaches.

soft X-ray lines in a quiescent active region. Subsequent observations following the *SMM* repair mission (Figure 20) confirm the earlier result that turbulent velocities of up to 100 km s^{-1} exist in active regions. The new data also seem to rule out

systematic upflows with velocities greater than 20 km s^{-1} (the FCS velocity sensitivity limit) and indicate that the greatest mass motions occur in the brightest areas of active region soft X-ray emission. These areas lie over the photospheric magnetic

SMM-FCS X-RAY AND OPTICAL IMAGES OF NOAA AR 4474

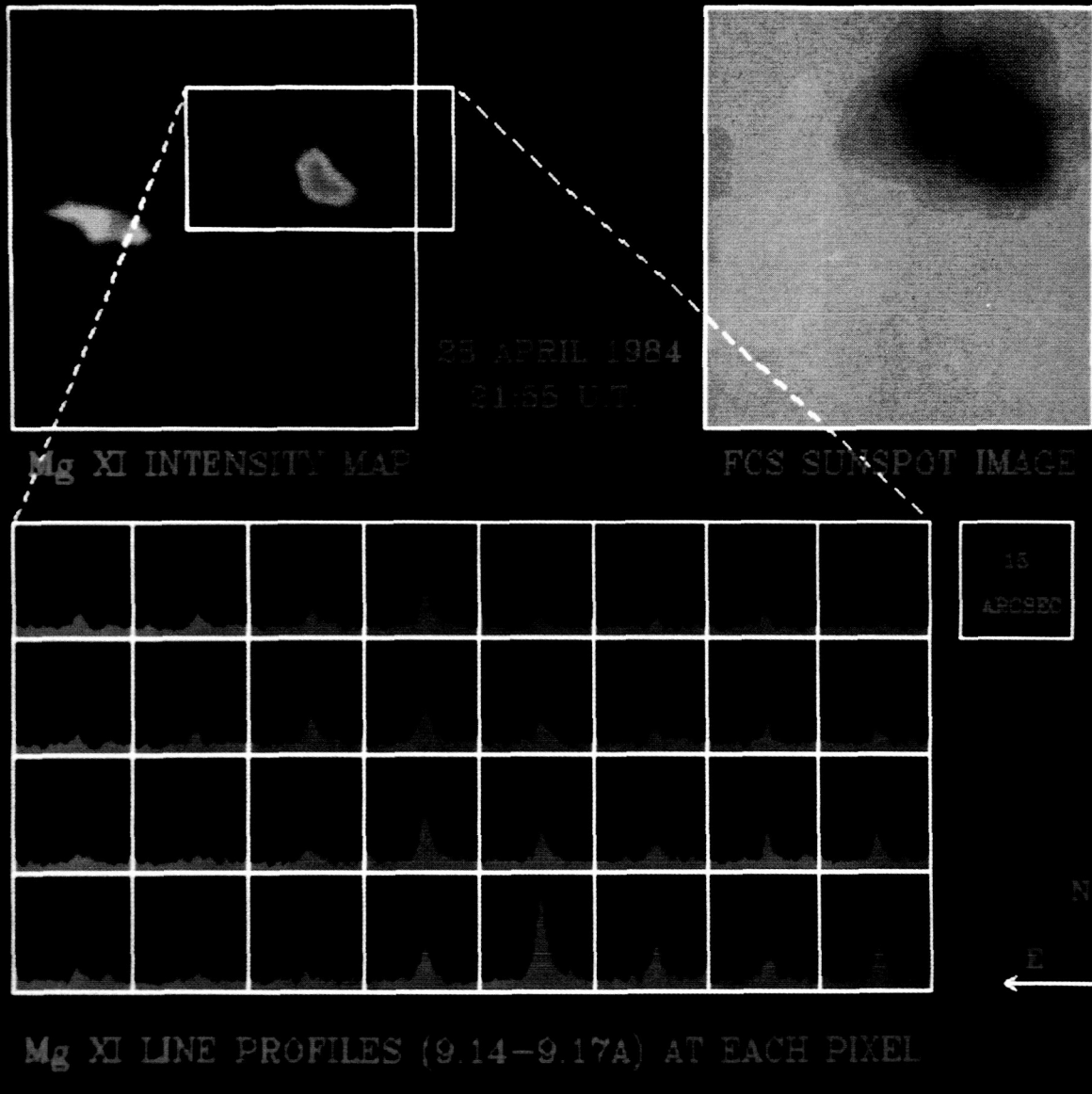


Figure 20. At the top left is a $3' \times 3'$ square false-color X-ray image of NOAA Active Region (AR) 4474 in the soft X-ray line of Mg XI at $\approx 9.16 \text{ \AA}$. Wavelength scans were made in the $2' \times 1'$ rectangular region, indicated by the white rectangle, around the brightest point. At the top right is the $3' \times 3'$ FCS sunspot image used for coalignment with ground-based data ($H\alpha$ and white light images from Learmonth Observatory and a Kitt Peak National Observatory magnetogram). The lower half of the figure shows Mg XI line profiles at each $15''$ square pixel in the rectangle. After correction for projection, the magnetic neutral line runs through the four brightest line profiles, which are also the broadest. The "excess width" above thermal broadening for these profiles corresponds to a turbulent velocity of 50 km s^{-1} .

"neutral line" (the boundary of fields of opposite polarity), and are therefore believed to be the tops of loops. In addition to placing constraints on models of active region and preflare coronal loop structure, observations of soft X-ray line broadening may eventually lead to an understanding of the mechanism that heats these arcades.

A program of observing this phenomenon in a number of different circumstances continues, and will be extended to look at other targets such as sunspots, plages, and filaments, to determine the range of variation of non-thermal broadening of soft X-ray lines in the solar atmosphere.

PROMINENCE OBSERVATIONS

UVSP has given us the ability to observe prominences at wavelengths, and hence temperatures, not seen from the earth and to measure the velocity of prominence material as a function of position and time. While there are several theories describing prominence formation and structure, we have not had the necessary observations to compare with these theories. The *SMM* observations in the ultraviolet have begun to give us some of the necessary data.

By using the UVSP spectral and imaging capabilities, Poland and Tandberg-Hanssen (1983) were able

to obtain images and line profiles in prominences over a wide range of temperatures in a relatively short period. Examples of these images are shown in Figure 21 where we present images in Ly α ($T \sim 10^4$ K), O IV ($\sim 1.8 \times 10^5$ K), Si IV ($\sim 8 \times 10^4$ K), C IV ($\sim 10^5$ K), He II ($\sim 3 \times 10^4$ K), and C I (~ 5000 K). It is clear from these images that the prominence structure varies with temperature. By obtaining photometric line profiles in each of these lines in prominences, we have also been able to determine lower limits to the turbulent line-broadening velocities.

Observations obtained in the Dopplergram mode allowed Schieder *et al.* (1985) to obtain velocity

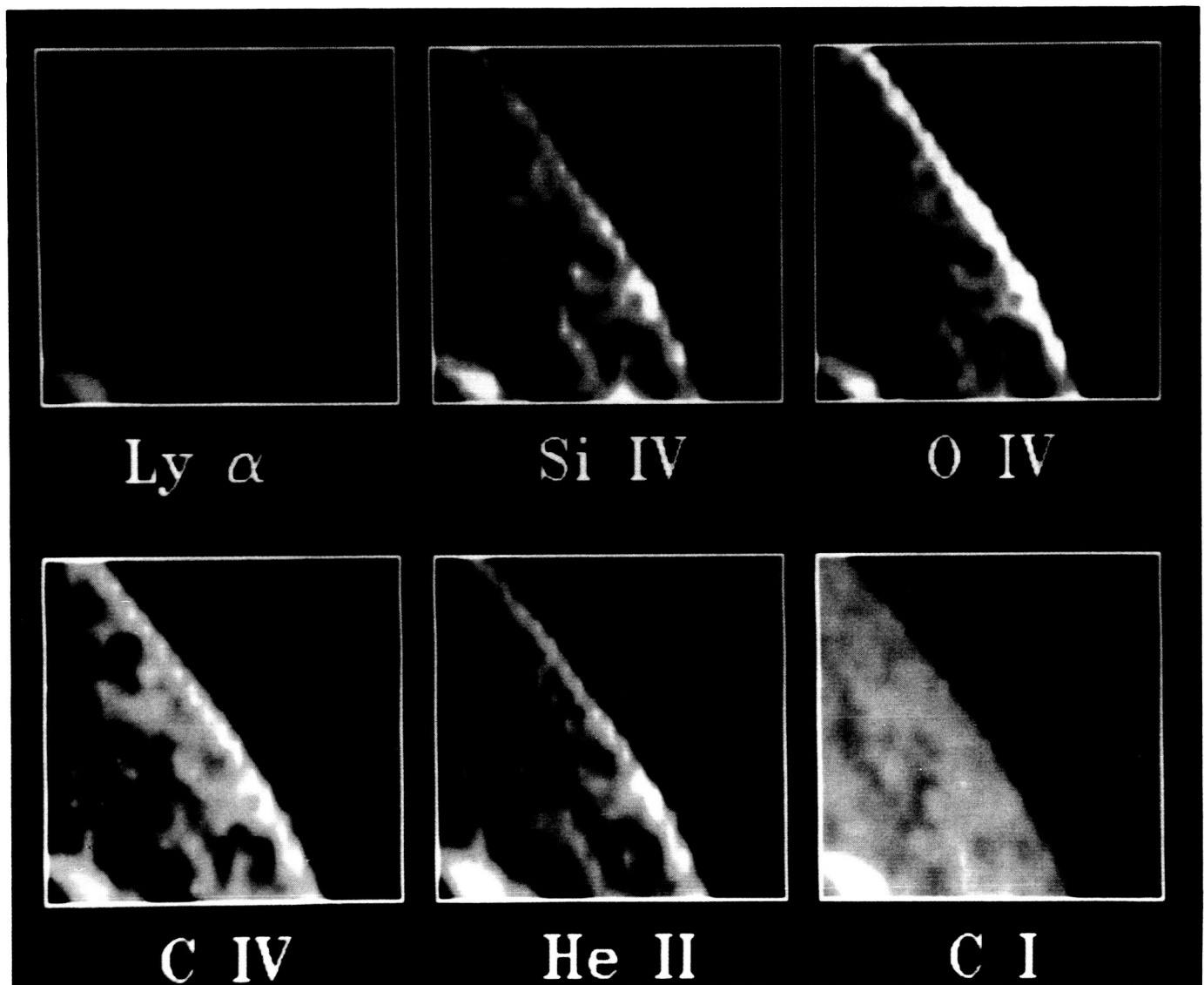


Figure 21. A series of UVSP spectroheliograms of the northwest limb of the Sun, including a quiescent prominence, on 20 November, 1980. The pixel size is $10'' \times 10''$, and the image size is $250'' \times 250''$. Clockwise from upper left, the images were obtained in H Ly α 1216 Å, Si IV 1402 Å, O IV 1401 Å, C IV 1548 Å, He II 1640 Å, and C I 1655 Å.

as a function of position and time in prominences. An example of this type of measurement in a disk filament is shown in Figure 22, where we plot velocity along the filament axis. These measurements, in active region filaments on the disk, show a downflow at the footpoints (marked A, B, C, and D in Figure 22) with an upward velocity between. The footpoints are also the regions of strongest photospheric magnetic field along the filament. This suggests a model of a long magnetic flux rope with material slowly draining out at the footpoints. As the total mass in the loop decreases it allows the central part to rise. Although this model seems observationally satisfying, the observed time scales are not in agreement with our current understanding of the expected plasma physics interactions, indicating that further theoretical work is needed.

SUNSPOTS

Some of the most intriguing observational results from UVSP have come from sunspots, and concern magnetic fields, mass flows, emission measure models, and wave propagation. Henze *et al.* (1982) used the UVSP polarimeter to obtain the first direct measurement of transition region magnetic field via the Zeeman effect. The longitudinal magnetic field strength in a $10'' \times 10''$ pixel over a sunspot umbra was approximately 1000 gauss, with a measurement uncertainty of roughly 100 gauss; the measurement was obtained in the 1548 \AA resonance line of C IV, formed at about 10^5 K . A photospheric magnetogram yielded an average value of approximately (1900 ± 70) gauss for the underlying $10'' \times 10''$ arc sec area of the same umbra. Comparing various

methods of estimating the magnetic field gradient over the same spot, Hagyard *et al.* (1983) found that a $\nabla \cdot \mathbf{B} = 0$ extension of the photospheric transverse field B_{\perp} , as measured by the Marshall Space Flight Center vector magnetograph, and a potential field extension of the photospheric B_{\parallel} , gave consistent values of $0.12 - 0.28 \text{ gauss km}^{-1}$. The transition region over the umbra, at least, thus appears to lie 4000 to 6000 km above the visible surface.

Examining the vertical velocity in C IV $\lambda 1548$ over a sample of eight umbrae, Gurman and Athay (1983) found only one spot with either a bright "plume" of the type observed by *Skylab* or a mean mass flow of either sense greater than 4 km s^{-1} ; it displayed a downflow of $(7.2 \pm 3.3) \text{ km s}^{-1}$, still much smaller than the supersonic transition region downflows observed by Nicolas *et al.* (1982) with HRTS. Since it is possible that the HRTS observations may have been complicated by the presence of a light bridge in the umbra, the subject of umbral mass flows bears further study.

Kingston *et al.* (1982) performed an emission measure analysis of two umbrae with lines formed at $4.4 < \log_{10} T_e < 6.3$. Their results depicted a sunspot transition region both hotter and more tenuous than the brighter, denser umbrae observed with *Skylab* by Foukal (1976) and Doyle *et al.* (1985). The discrepancy may be resolved if the umbral transition region consists of filamented regions of both hot, tenuous material, and cooler, denser material.

Due to the length of the *SMM* orbital day, and the spatial and spectral resolution of UVSP, Gurman *et al.* (1982) were able to detect intensity and velocity oscillations at frequencies of $5.8 - 7.8 \text{ mHz}$ in transition region lines above sunspot umbrae that had escaped the notice of earlier satellite and

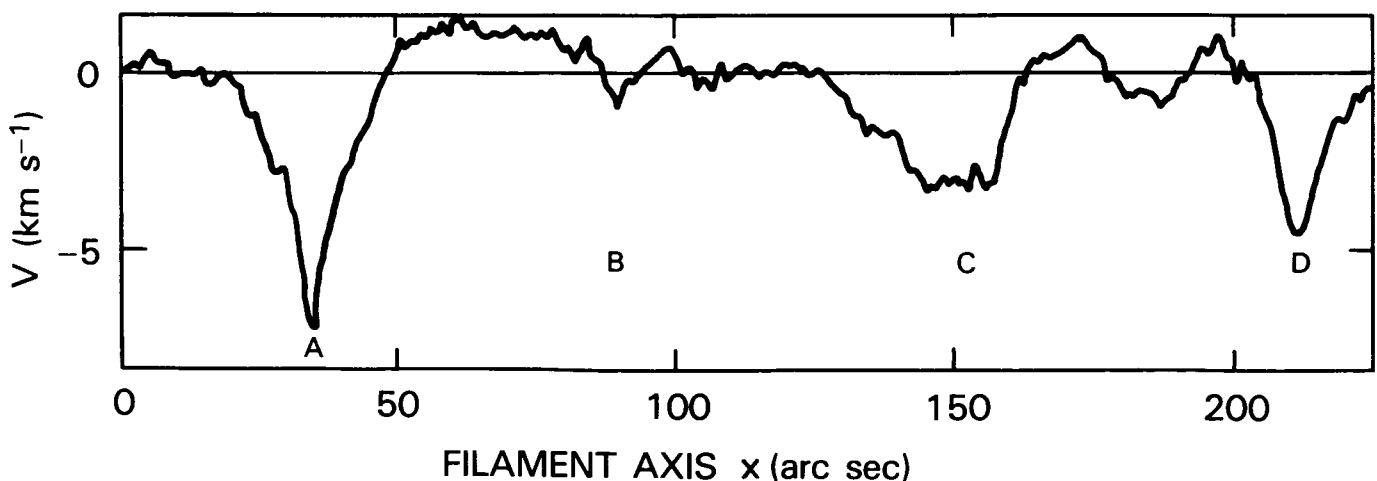


Figure 22. Velocity measured in the resonance line of C IV at 1548 \AA in the ultraviolet along a filament. Note the downward motion at footpoints A, B, and C and the smaller, upward velocities between them.

rocket-borne ultraviolet instruments. The intensity-velocity phase relation and amplitude of these oscillations leaves no doubt that they are upward-propagating acoustic waves. Some disagreement still exists between models interpreting the umbral oscillations in terms of an acoustic wave leakage from a subphotospheric cavity trapping magnetohydrodynamic waves (e.g. Thomas 1984) and those describing the observations in terms of the resonant transmission of magnetoacoustic waves by a chromospheric cavity (Žugžda, Locans, and Staude 1983; Gurman and Leibacher 1984), but it seems likely that both cavities play a part in the modulation of wave flux in the umbral atmosphere.

References

- Acton, L. W. *et al.* 1981, *The Astrophysical Journal*, 244, L137
- Doyle, J. G., Raymond, J. C., Noyes, R. W., and Kingston, A. E. 1985, *The Astrophysical Journal*, 297, 816
- Foukal, P. 1976, *Ap. J.*, 210, 575
- Gurman, J. B. and Athay, R. G. 1983, *The Astrophysical Journal*, 273, 374
- Gurman, J. B. and Leibacher, J. W. 1984, *The Astrophysical Journal*, 283, 859
- Gurman, J. B., Leibacher, J. W., Shine, R. A., Woodgate, B. E., and Henze, W. 1982, *The Astrophysical Journal*, 253, 939
- Hagyard, M. *et al.* 1983, *Solar Physics*, 84, 13
- Henze, W. *et al.* 1982, *Solar Physics*, 81, 231
- Hundhausen, A., Sawyer, C., House, L. L., Illing, R., and Wagner, W. 1984, *Journal of Geophysical Research*, 89 (A5), 2639
- Hundhausen, A. 1987, in preparation
- Kingston, A. E., Doyle, J. G., Dufton, P. L., and Gurman, J. B. 1982, *Solar Physics*, 81, 47
- Nicolas, K. R., Kjeldseth-Moe, O., Bartoe, J.-D. F., and Brueckner, G. E. 1982, *Solar Physics*, 81, 253
- Poland, A. and Tandberg-Hanssen, E. 1983, *Solar Physics*, 84, 63
- Schmieder, B., Malherbe, J.-M., Poland, A. I., and Simon, G. 1985, *Astronomy and Astrophysics*, 153, 64
- Simnett, G. M. and Harrison, R. A. 1985, *Solar Physics*, 99, 291
- Steinolfson, R. 1987, in preparation
- Thomas, J. H. 1984, *Astronomy and Astrophysics*, 135, 188
- Žugžda, Y. D., Locans, V., and Staude, J. 1983, *Solar Physics*, 82, 369

NON-SOLAR TARGETS

During January and February, 1986, C/P was able to obtain observations of Halley's Comet at times just before and after perihelion when scattered light from the Sun prevented ground-based observations. These observations were a delicate and demanding task for the C/P and spacecraft operations teams, since neither the instrument nor *SMM* was designed for pointing at targets other than the Sun. This activity was carried out as part of the worldwide International Halley Watch, specifically to determine whether tail disconnections occurred as the comet passed through sector boundaries in the interplanetary extension of the Sun's magnetic field.

While the GRS is unable to pinpoint the location of solar flares without correlative data from other, spatially resolved observations, its broad field of view (nearly half the sky) is an advantage in observing cosmic γ -ray sources while the spacecraft points at the Sun. Using GRS data, Matz *et al.* (1985) found that strong emission at energies above 1 MeV is a common property of cosmic γ -ray bursts, contrary to earlier predictions based on thermal fits to data at energies lower than 500 keV and the expectation that pair-production opacity at higher energies would strongly attenuate ≥ 1 MeV photons at the source. The high energy emission places strong constraints on models of γ -ray bursters, and the generation of such emission is currently a central theoretical issue in γ -ray burst astrophysics. Since GRS is currently the only instrument capable of measuring > 1 MeV emission from cosmic bursts, the continued operation of *SMM* is of great interest to γ -ray astrophysicists as well as solar physicists.

On 5 August, 1984, the GRS detected an intense γ -ray burst from the constellation Hydra. Spectra from three 16.38 s intervals during the burst (Figure 23), are very similar, as are spectra with lower energy resolution obtained every 2 s; this similarity suggests that the observed spectral shape may be fundamental to bursts. This result is consistent with measurements of weaker bursts made earlier with the GRS, and is of particular interest because the spectral shape cannot be reconciled with thermal processes alone: new physical models are required to explain the hard spectra extending to energies above 10 MeV on timescales as short as seconds.

Despite a somewhat narrower field of view than that of GRS, HXRBS has also detected several non-solar γ -ray bursts within 40° of the direction to the Sun. The 5 August, 1984 event observed by GRS was found to be periodic (at the 99.4% confidence level), at 2.2 s in HXRBS shield data

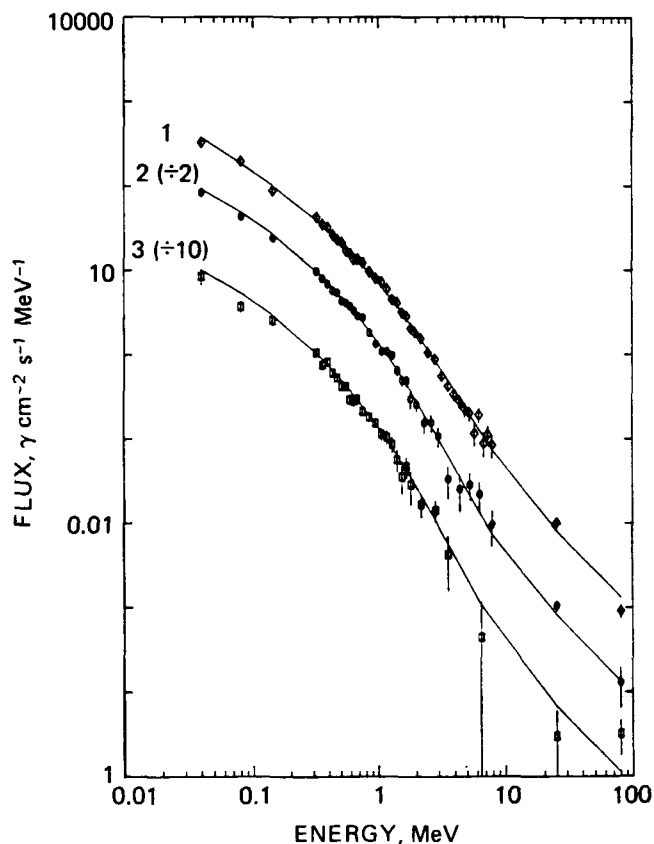


Figure 23. GRS γ -ray spectra from three 16.38 s intervals during the cosmic burst of 5 August, 1984. The shape of these and other cosmic burst spectra indicate a definitely nonthermal origin for the burster γ -rays.

($\sim 120 - 130$ keV). Analysis of other HXRBS observations led to the first identification of spectral evolution, from hard to soft, in conventional bursts (Norris *et al.* 1986), and the discovery of the so-called soft γ -ray repeater SGR 1806-21 (Atteia *et al.* 1987, Laros *et al.* 1987). These soft bursts have somewhat steeper spectra than normal gamma-ray bursts, and at least one event, apparently from close to the galactic center, shows rise and fall times shorter than the 5 ms time resolution, with an overall duration of only 45 ms (Kouveliotou *et al.* 1986). Triangulation of data from *SMM*, *ISEE-3*, *Pioneer Venus Orbiter*, and the Soviet *Prognoz* and *Venera* spacecraft yield the same location for all the common bursts. A particularly exciting aspect of a repeating burster is that ground-based radio and optical telescopes, as well as future X-ray and gamma-ray imaging devices, can be trained onto the triangulated location, with a good prospect of detecting bursts simultaneously at different energies.

Each winter, the *SMM* solar pointing sweeps GRS across the galactic center. By differencing data from these periods and periods six months apart (when GRS is able to sample the galactic anticenter), Share *et al.* (1985) found a strong emission line from the galactic center at 1.804 ± 0.004 MeV, with an intrinsic full width at half-maximum of 38 ± 21 keV (Figure 24). This is consistent with a narrow emission line at 1.809 MeV from interstellar ^{26}Al . This is only the second unambiguously identified γ -ray line observed from a source outside the solar system and is probably a tracer for the presence of

evolved objects that would expel significant amounts of nuclei as massive as ^{26}Al , such as red giants and Wolf-Rayet stars.

Currently, the GRS data are being analyzed for evidence of other cosmic γ -ray sources such as SS433 and transient lines emission from early phases of galactic novae. In addition, GRS data have been found to show a significant increase in the intensity of the 0.511 MeV line radiation in each of the years it has been observed in the region of the sky about the galactic center. The time-averaged flux for a point source at the galactic center would be $\sim 2.2 \times 10^{-3}$ photons $\text{cm}^{-2} \text{s}^{-1}$, but it is more likely that the γ -ray flux arises from positron annihilation over an extended area along the galactic plane. Since positrons in the interstellar medium have half-lives against annihilation of $\sim 10^5$ years, the sources of the 0.511 MeV radiation must have similar or longer lifetimes. Possible candidate sources of interstellar positrons therefore include radioactive nuclei produced in the more advanced stages of stellar evolution, such as supernovae and red giants.

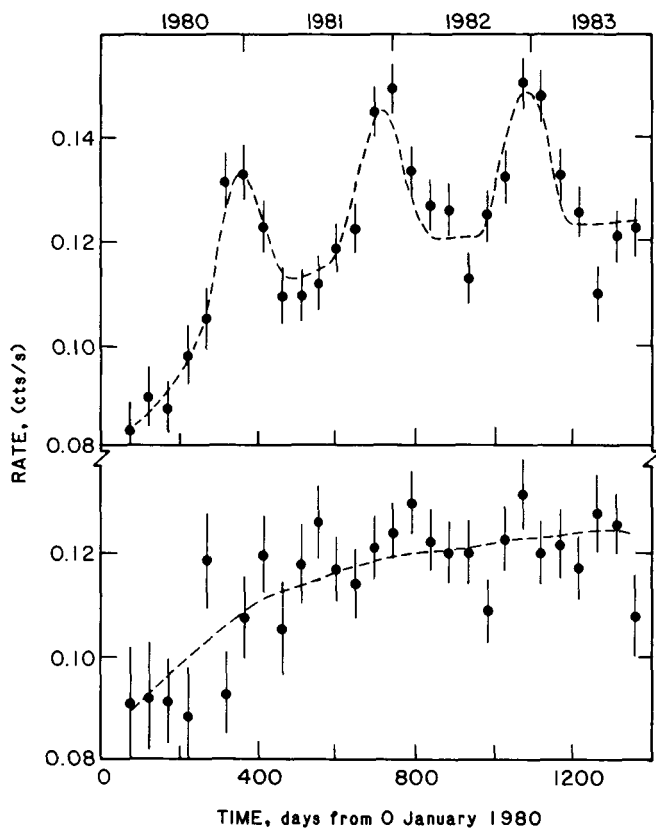


Figure 24. ^{26}Al γ -ray line strength when (top) *SMM* is pointing toward the sky, and (bottom) the field of view is blocked by the earth. The yearly peaks correspond to times when *SMM* is pointing in the direction of the galactic plane.

References

- Atteia, J.-L. *et al.* 1987, submitted *Astrophysical Journal Letters*
- Kouveliotou, C. *et al.* 1986, *Advances in Space Science*, 6, 4
- Laros, J. *et al.* 1987, submitted *Astrophysical Journal Letters*
- Matz, S. M., Forrest, D. J., Vestrand, W. T., Chupp, E. L., Share, G. H., and Rieger, E. 1985, *The Astrophysical Journal*, 288, L37
- Norris, J. P., Share, G. H., Messina, D. C., Cline, T. L., Desai, U. D., Dennis, B. R., Matz, S. M., and Chupp, E. L. 1986, *The Astrophysical Journal*, 301, 213
- Share, G. H., Kinzer, R. L., Kurfess, J. D., Forrest, D. J., Chupp, E. L., and Rieger, E. 1985, *The Astrophysical Journal*, 292, L61

FUTURE PLANS

At this writing, *SMM* instruments are observing the beginning of a new solar cycle. In October, 1986, data were obtained on several flares from active regions at solar latitudes of 20° to 30° . The high latitudes are indicative of the early phase of a solar cycle, as known from the so-called "butterfly" diagram. Also associated with these new-cycle regions was a significant resurgence of coronal activity: a coronal mass ejection was observed by the Corona-graph/Polarimeter on 15 October, 1986 with a radial velocity of over 600 km s^{-1} (see Figure 25). This is significantly greater than the typical CME velocity ($\sim 200 \text{ km s}^{-1}$) in the period of solar minimum (April, 1984 - September, 1986). This event tends to confirm the view of the flare-CME association described in the section on The Active Solar Atmosphere: Both an X-ray flare and a flare spray were associated with a large CME, and both occurred well off to one side of the ejection. Both the mass ejection, a typical, bright, frontal loop followed by a dark, interior cavity, and the flare spray, still emitting the $H\alpha$ were seen in the C/P field of view. The spray was located near one side of the dark cavity, and later, strands of $H\alpha$ -emitting material ejected from the flare site appeared to move non-radially and fill the expanding cavity. Finally, a set of compact post-flare loops developed at the (off-center) site of the initial flare spray.

As the solar cycle enters a new phase, the non-solar capabilities of *SMM* are being stretched as well. Beginning in December, 1986, *SMM* investigators attempted to point the spacecraft away from the Sun for periods of one to three hours to measure hard X-ray and γ -ray spectra from Cygnus X-1, the leading black hole candidate. Radical changes in the shape of the hard X-ray and γ -ray spectrum of Cyg X-1 have been observed in the past by *HEAO-3* instruments, and until the March, 1987 launch of the Japanese *Ginga* spacecraft, the *SMM* HXRBS and GRS were the only orbiting instruments currently capable of monitoring these changes over an extended period.

More recently, supernova 1987a in the Large Magellanic Cloud has given astronomers the opportunity to study the violent, late phase of the evolution of massive stars in a relatively nearby object - closer, in fact, than any other supernova since the invention of the telescope. Although this supernova appears to be fairly peculiar, even by supernova standards, models of similar events predict that the shell of stellar matter thrown off in the initial explosion will thin sufficiently in several months to allow the escape of γ -rays emitted in the radioactive decay of heavy nuclei present in the supernova. Since the *SMM* GRS is the only orbiting γ -ray instrument likely to be sensitive enough to detect this emission, the GRS team hopes to be able to provide an early warning that will trigger the launch of air-, balloon-, and sounding rocket-borne instruments to study the new supernova remnant in detail.

A significant share of the scientific harvest reaped by *SMM* has been the result of research funded by the *SMM* Guest Investigator program. This program continues to be well supported by NASA, with 20 to 25 new programs expected to be approved for the coming year. Guest Investigators are encouraged to work closely with Principal Investigator team members, and such collaborations have proven extremely valuable in expanding the base of the *SMM* user community. Interested, qualified investigators should contact Dr. David Bohlin, Code EZ, at NASA Headquarters. This year, a new, multi-disciplinary Space Astrophysical Data Analysis Program (SADAP) will provide support for research on archival data from many recent space astronomy missions, including *SMM*. Any investigator interested only in *SMM* data more than one year old (and therefore in the public domain) should also contact Dr. Bohlin.

Even as its lifetime extends toward the beginning of a new solar maximum, NASA's *Solar Maximum Mission* continues to provide data that will challenge the ingenuity of the astrophysical community for years to come as we try to understand a new Sun.

(Figure 25 on Reverse)

ORIGINAL PAGE
COLOR PHOTOGRAPH

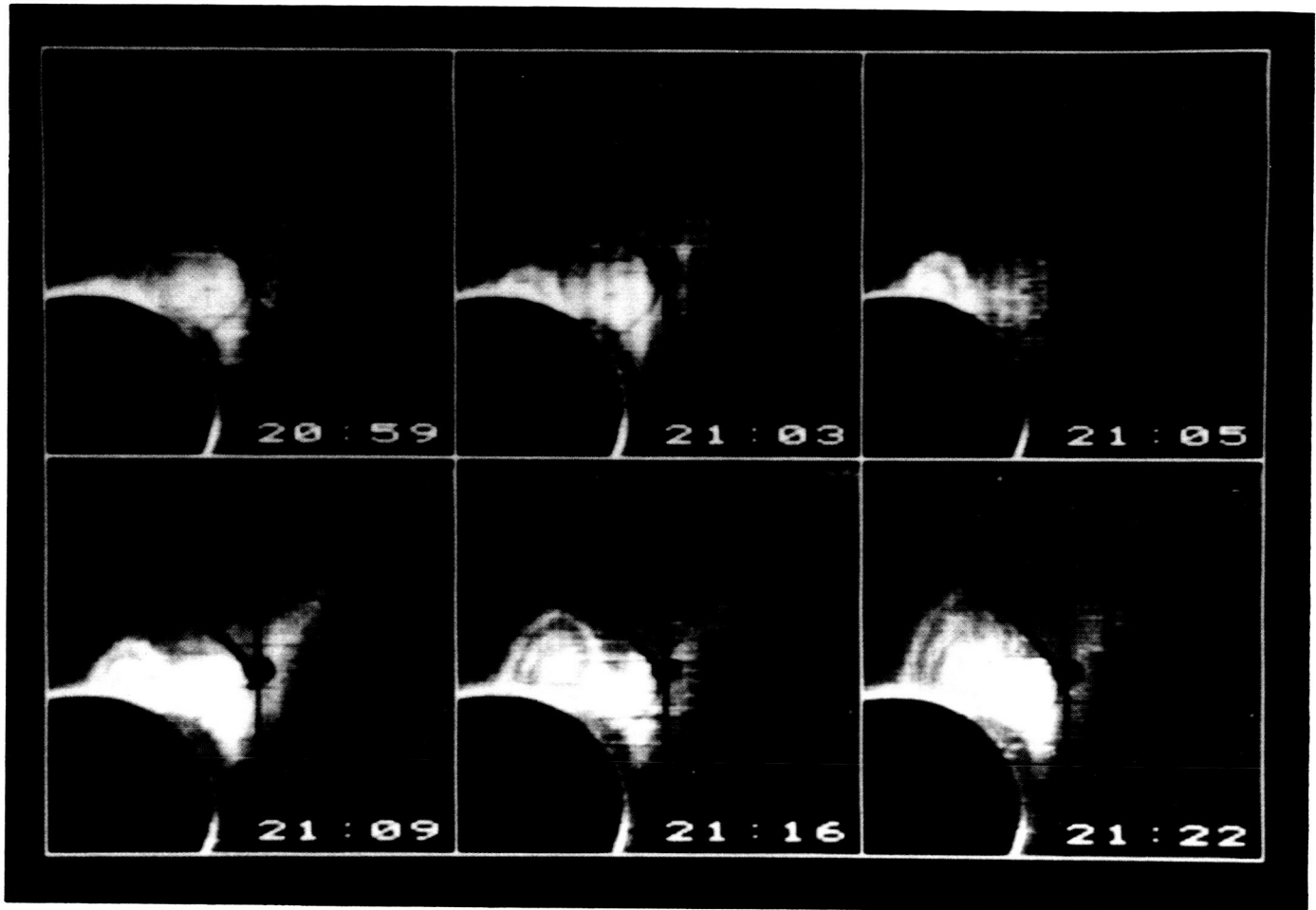


Figure 25. A time series of quick-look images of a high-latitude coronal mass ejection associated with an active region from the new solar cycle 22, on 15 October, 1986. The front of the ejection is moving at $\approx 670 \text{ km s}^{-1}$. This event was triggered by a prominence eruption that was well observed by a ground-based coronagraph.

BACK COVER PHOTOGRAPH:

The *Solar Maximum Mission* spacecraft in orbit after its retrieval, repair, and redeployment - the first ever of an orbiting spacecraft - by the crew of the Space Shuttle *Challenger* in April, 1984.



NASA

National Aeronautics and
Space Administration

Goddard Space Flight Center